REVIEW

Recent progresses in the single-atom catalysts for the oxygen reduction reaction

Yalong Li[1] · Xiaolong Xu[1] · Zizheng Ai[1] · Baoguo Zhang[1] · Dong Shi[1] · Mingzhi Yang[1] · Haixiao Hu[1] · Yongliang Shao[1] · Yongzhong Wu[1] · Xiaopeng Hao[1]

Abstract

The development of high-performance electrocatalysts is critical for the widespread applications of the sustainable energy technologies. In this context, single-atom catalysts (SACs) with isolated metal sites have attracted more attention because of their maximum atom utilization and remarkable electrocatalytic performance. However, the high surface energy often results in a low loading of the single metal atoms, limiting their practical applications. Herein, we give an up-to-date review on the progress for the SACs. The research progress of noble metal SACs, transition metal SACs, single-atom alloy SACs, and double metal SACs is summarized. The advantages and disadvantages of synthesis strategies including wet chemistry, atomic layer deposition, and high-temperature pyrolysis are discussed. We also propose some new research direction to obtain the high-performance SACs. It is expected to realize widely applications of SACs.

Keywords Electrocatalysts · Oxygen reduction reaction · Single-atom catalysts · Synthetic approaches · Research direction

Introduction

Many energy conversion techniques (such as metal–air batteries) have been developed with the energy consumption and climate warming [1–4]. The development of high-performance electrocatalysts is crucial to meet above techniques, focusing on facilitating kinetics and lowering the energy barrier during the electrocatalytic processes [5, 6]. Figure 1a is the mechanism diagram of metal air battery, from which we can see oxygen reduction reaction (ORR) is an important cathode reaction in the discharge processes of metal–air batteries [7]. Based on Fig. 1b, the ORR on N-doped carbon materials working principles is described for two possible pathways [8]. One is the four-electron mechanism taking place at a single site: The protons attach to the two oxygen atoms, leading to breakage of the O–OH bond and formation of OH species; the additional proton then reacts with the adsorbed OH to

form H_2O. The other is the $2+2$-electron mechanism, which does not always take place at a single site; H_2O_2 is formed by reaction of the adsorbed OOH species with another proton, followed by reabsorption of H_2O_2 and its reduction by two protons to generate H_2O. For metal–air batteries, ORR favors the four-electron process. Therefore, the electrocatalysts with four-electron mechanism have become the research hotpot.

Up to now, single-atom catalysts (SACs) have attracted more attention in the field of electrocatalysis. The catalytic activity and selectivity toward electrochemical reactions can be obviously increased through downsizing the metal nanoparticles into single atoms [9]. However, their high surface free energies make them easy aggregation; thus, it requires various substrates to form a stable configuration for the isolated atoms [10]. The dispersion of metal atoms in SACs not only favors the catalytic activity and selectivity during the electrocatalytic processes, but also reduces costs and increases atom utilization [11]. The catalytic performance of SACs can be enhanced via the tunable electronic structures formed by the strong interactions between the substrates and the individual atoms [12]. Unsaturated coordination environments of SACs play a critical role in the adsorption and activation of reactants, profiting to lower the energy barrier for electrochemical reactions [13].

The noble metals of platinum (Pt) have been used as ORR electrocatalysts. For example, Lai et al. [14] reported a

✉ Xiaolong Xu
  xlxu@qlu.edu.cn

✉ Yongzhong Wu
  wuyz@qlu.edu.cn

1 School of Materials Science and Engineering, Qilu University of Technology (Shandong Academy of Sciences), Jinan 250353, China

Fig. 1 **a** Schematic of a rechargeable zinc air flow battery [7]. Copyright 2021, Elsevier. **b** Schematic pathway for the ORR on N-doped carbon materials [8]. Copyright 2016, Science
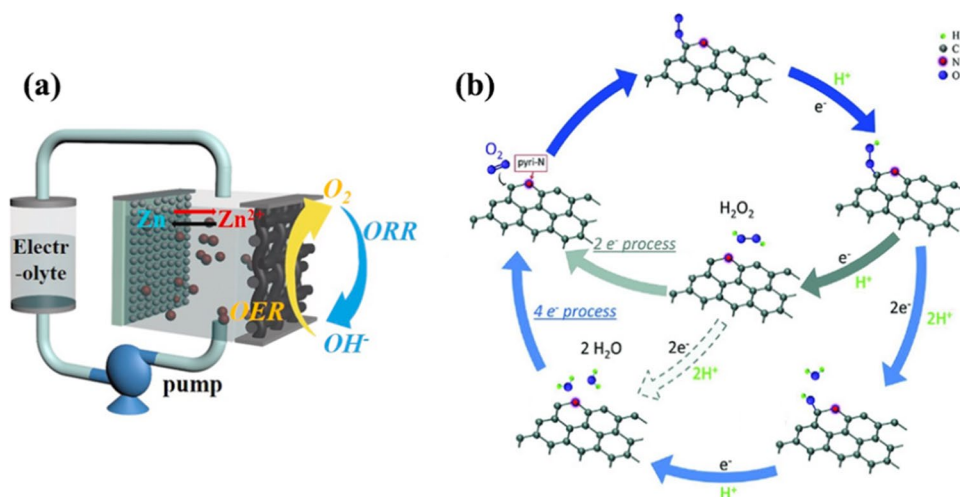
quasi-Pt-allotrope SAC, increasing the efficiency of the ORR in virtue of the isolated Pt atoms. However, their high cost and unsatisfactory durability hinder their applications. Consequently, the development of transition metal-based catalytic systems for ORR is necessary [15]. For instance, Co single atoms dispersed on porous N-doped carbon nanotube (Co-NCNT) showed an ORR half-wave potential ($E_{1/2}$) of 0.87 V, outperforming that of Pt/C (20 wt%) [16]. At the same time, the single-atom alloy SACs formed by alloying different single atoms also show good catalytic potential. Such as Xu et al. [17] synthesized FeCo alloy SAC, exhibiting an $E_{1/2}$ of 0.89 V. Furthermore, the double-metal SACs (DMSACs) formed by introducing a second metal atom presented more catalytic sites, exhibiting better electrocatalytic performance [18, 19]. For instance, Han et al. [20] reported a DMSACs with Co/Ni in N-doped carbon nanotubes, delivering an $E_{1/2}$ of 0.76 V and an onset potential (E_{onset}) of 0.88 V. Furthermore, Guo et al. [21] gave a review on the progress of approaches for the synthesis of SACs, outline the general principles and list the advantages and disadvantages of each synthesis approach. Gawande et al. [22] collected the latest advances concerning the applications of SACs in the ORR. However, there is still a lack of a comprehensive overview of the latest developments in ORR SACs. It is necessary to summarize systematically the classification and preparation methods of SACs to give the readers a clear picture and inspire more studies to exploit novel approaches.

In this review, we summarized the research progress of noble metal SACs including Pt–N–C, Pd–N–C, Pt–O–C, and Pt–C; transition metal SACs including Fe–N–C, Fe–O–C, Co–N–C, Ni–N–C, Cu–N–C, Zn–N–C, and Mn–N–C; single-atom alloy catalysts including Pt–M (Pd, Fe, Co) and Pd–M (Ag, Ir, Co, Ni); as well as double metal SACs including Pt/Ni–N–C, Fe/Ni–N–C, and Fe/Co–N–C (Fig. 2). Moreover, the synthesis approaches for SACs including wet chemistry, atomic layer deposition, and high-temperature pyrolysis were discussed. Moreover, the new research directions of
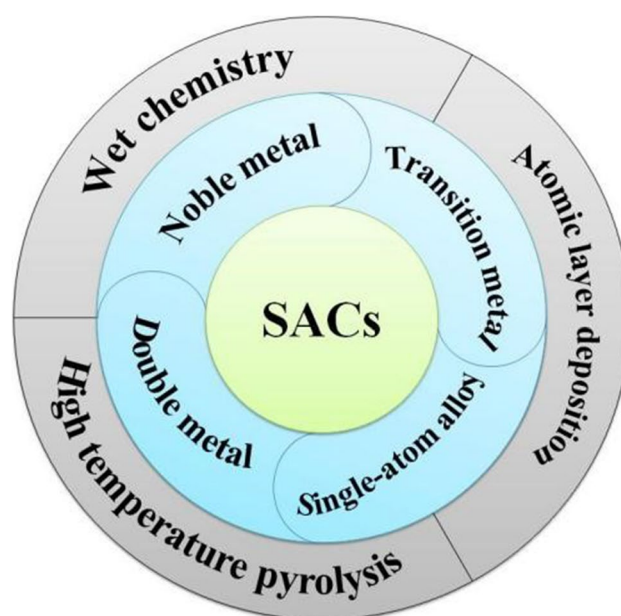
Fig. 2 Review scheme of SACs

SACs were proposed, such as improving the dispersion and loading of metal active centers, exploring suitable carriers and clarifying the synergistic mechanism between metal atoms in SACs.

Classification

Noble metal SACs

Due to the high activity and selectivity, the noble metal catalysts have been used for ORR [23, 24]. We discussed the progress of Pt–N–C and Pd–N–C in the research of ORR electrocatalysts (Tables 1 and 2).

Pt–N–C

Pt–N–C has high ORR catalytic activity in alkaline medium [71]. However, the commercial value of Pt is significantly hindered by its low abundance, limited supplies. Accordingly, many researches focus on increasing Pt catalytic activity such as E_{onset}, $E_{1/2}$, and limiting current density (J_L) [72–74]. Recently, Pt supported on heteroatom-doped carbon, even the Pt–N–C, has been reported to improve ORR performance with long-term stability [75]. As a case, Zhao et al. [25] synthesized Pt–N–C supported on g-C$_3$N$_4$ nanosheets (Pt-CNHS) via the liquid-phase reaction of g-C$_3$N$_4$ and H$_2$PtCl$_6$ (Fig. 3a1-2), showing an E_{onset} of 3.7 V. Lai et al. [64] distributed Pt atoms on a heterogeneous substrate formed by Co particles and N-doped carbon frameworks (Pt@Co/NC; Fig. 3b1). The Pt@Co/NC delivered a mass activity is 4.2 mA μg_{Pt}^{-1} at 0.9 V (that of Pt/C is 0.15 mA μg_{Pt}^{-1}) and a mass activity of 6.2 mA μg_{Pt}^{-1} at 0.85 V (that of Pt/C is 0.48 mA μg_{Pt}^{-1}; Fig. 3b2). Xiang et al. [65] reported a carbon-supported Pt–N–C (Pt–N$_4$–C) prepared using a small molecular Pt complex containing moieties as the Pt precursor. It showed high ORR performance with the activity of 0.108 mA μg_{Pt}^{-1} at 0.9 V (that of 20 wt% Pt/C is 0.035 mA μg_{Pt}^{-1}). Moreover, adjusting N coordination is an effective method to improve the catalytic performance. Fan et al. [26] proposed a research model of Pt–N$_x$–C structure ($1 \leq x \leq 4$) fabricated by a zeolitic imidazolate framework (ZIF)-8 template (Fig. 3c1). The results showed the catalytic activity gradually increases with the decrease of x value, especially the positive E_{onset} (1.10 V; Fig. 3c2).

Pd–N–C

Pd–N–C has emerged as a potential alternative to Pt–N–C for ORR due to the high selectivity and lower costs compared with Pt [76]. Different supports can significantly alter the catalytic performance of Pd catalysts [77, 78]. In this aspect, Wang et al. [79] reported Pd–N–C SACs (Fig. 4a1) derived from Pd-doped ZIFs through one-step thermolysis. The catalyst exhibited about 95% selectivity toward H$_2$O$_2$ (Fig. 4a2) and an E_{onset} of 0.8 V. Xiang et al. [27] developed a strategy to deposit Pd atoms on MnO$_2$ nanowires and carbon nanotubes (Pd/MnO$_2$-CNT). The Pd–N–C had an E_{onset} of 0.982 V. Jin et al. [66] immobilized Pd atoms on thin layers of graphitic carbon nitride with carbon black (C@C$_3$N$_4$) to produce the Pd–N–C. It showed that the current density increased with the Pd content increased (Fig. 4b1). The Pd–N–C showed very high selectivity for H$_2$O$_2$ production up to 94% (Fig. 4b2). Furthermore, one or a few layers of atoms in Pd–N–C films could minimize the use of Pd atoms and enhance their performance [80].

Others

Other noble metals such as Au–N–C, Ag–N–C, Ir–N–C, Pt–C, and Pt–O–C can also improve ORR performance to some extent. For instance, Fortunato et al. [81] reported an Au–N–C is constructed using Au–Pd molybdenum oxide supported on graphene nanoribbons. The catalysts exhibited high catalytic activity ($E_{onset} = 0.72$ V) and selectivity for H$_2$O$_2$ (75%). Cartagena et al. [82] prepared the Ag–N–C by using the rotating disk slurry electrode technique. The most ORR mass activities Ag–N–C (0.1 V, 4,765,000 mA μg^{-1}) demonstrated three times higher activity than the least active one (0.4 V, 1,637,000 mA μg^{-1}). Xiao et al. [83] developed an Ir–N–C, which mimics homogeneous iridium porphyrins for ORR catalysis. The Ir–N–C showed a mass activity of 12.2 mA μg^{-1} at 0.85 V. Xu et al. [84] synthetized Pt–C with an $E_{1/2}$ of 0.85 V. Roh et al. [85] synthetized Pt–O–C by controlling the hydrophilicity of carbon supports in the electrodes by functionalizing the carbon with oxygen-containing groups, showing an ECSA of 88 m^2 g_{Pt}^{-1}.

Transition metal catalysts

Transition metal ORR catalysts represent promising alternatives to noble metal catalysts owing to their high activity and high thermal stability [86–88]. Herein, the recent research progress of SACs, including Fe–N–C, Fe–O–C, Co–N–C, Ni–N–C, Cu–N–C, Zn–N–C, and Mn–N–C, was summarized for ORR (Tables 1 and 2).

Fe–N–C and Fe–O–C

Due to excellent adsorption capacity and good electrical conductivity, Fe has become a hot spot in monatomic catalysts [89]. Fe has a large number of filled 3d orbitals and different coordination structures, which makes it more possible to form SACs [90]. At present, in a large number of studies, four active sites of Fe SACs, Fe–N$_x$ [91], Fe–N$_2$ [92], Fe–N$_4$ [93] and Fe–N$_6$ [94], have been mainly studied. However, the traditional synthesis methods of Fe catalysts expose few active sites, and the catalytic performance is not ideal [95]. Therefore, the simple and efficient synthesis of monatomic Fe catalysts with high active sites has become the main direction.

Many methods (gas-phase fluorination-assisted method, one-pot method) to improve its ORR performance have been reported. For an instance, Meng et al. [28] prepared a Fe–N$_x$ on single-walled carbon nanotube (SWCNT) by gas-phase fluorination-assisted method (Fig. 5a1). The reduction potential reached 0.93 V at -3 mA cm^{-2}, which is better than that of Pt/C (0.86 V; Fig. 5a2-3). The confined nanopores can promote the activity and stability of ORR catalysts. Therefore, Cai et al. [29] designed a nanoporous Fe/N-doped

Table 1 Comparative ORR performance of various SACs in alkali solution

Type	Name	Full name	Synthesis method	Loading amount of metal (wt%)	E_{onset} (V)	$E_{1/2}$ (V)	J_L (mA cm^{-2})	Tafel slope (dec^{-1})	Stability — Current retention (%)	Shift of reduction potential (mV)	Refs
Noble metal SACs	Pt–N–C	Pt-CNHS	Liquid-phase reaction	0.77	3.7	-	-	-	69	-	[25]
		Pt–N$_x$–C	Pyrolysis	1.5	1.10	0.72	-	84.3	-	-	[26]
	Pd–N–C	Pd/MnO$_2$-CNT	ALD	0.68	0.982	0.947	-	-	-	-	[27]
Transition metal SACs	Fe–N–C	SAFe-SWCNT	Gas-phase fluorination-assisted method	-	1.04	-	14	66	-	-6	[28]
		Fe-NPC	One-pot method	-	0.971	-	6.55	-	82	-	[29]
		Fe–N–C/N-OMC	Pyrolysis	2.9	1.08	0.93	8.14	75	-	-	[30]
		FeZ8NC and NaCl	Molten-salt-assisted thermal emitting approach	0.42	-	0.896	-	42	-	-	[31]
		Fe–N$_x$–C	Pyrolysis	-	1.05	0.91	5.44	69	59.6	-	[32]
		Fe–N$_4$/NCs	Ultrasonic plasma engineering	0.29	0.92	0.80	-	65	83.6	-	[33]
	Fe–O–C	Fe–O–C	Graphene-assisted wet chemical route	-	1.00	0.92	-	50	97	-	[34]
	Co–N–C	Co–N/C–SAC	Pyrolysis strategy assisted by molten salts at high temperature	3.1	0.81	0.83	5.5	60.9	-	-	[35]
		Co–N-CCNFMs	Integrated core–shell electrospun	-	-	0.84	5.22	92.5	95	-	[36]
		NMCS-rGO-Co	Self-assembly method and pyrolysis strategy	1	-	0.82	-	74.2	79.4	-	[37]
		Cop@CoNC	Pyrolysis	3.82	0.94	0.84	-	37	-	-	[38]
	Ni–N–C	Ni SAs-NC	Secondary single-atom modulation strategy	1.57	-	0.854	-	56	-	-	[39]
		Ni–N–C	CVD	23	0.984	0.859	-	59	96	-	[40]
		Ni–N–CNT	One-pot pyrolysis method	20.03	0.88	0.75	-	-	-	-	[41]
	Cu–N–C	Cu–N–C SAC	Pyrolysis	2.0	-	0.83	5.25	37	90	-	[42]
		Cu SAs/NC-900	Ionic exchange strategy	-	-	0.87	-	79	-	-	[43]
		Cu/G SAC	Confined self-initiated dispersing protocol	5.4	-	0.85	3.787	-	-	-10	[44]
	Zn–N–C	A–Zn@NSG	Pyrolysis	1.02	1.040	0.905	6.35	39.64	-	-	[45]
		SA–Zn–NHPC	Solvothermal	-	0.85	0.78	4.71	-	-	-	[46]
		Zn–N–C	Pyrolysis	9.33	-	0.873	-	-	-	-18.67	[47]
		Zn–B/N–C	Pyrolysis	2.4	-	0.886	-	50	97	-	[48]
	Mn–N–C	Mn–SA	Pyrolysis	1.8	-	0.87	-	-	-	-	[49]
		PT-MnN$_4$	Bio-mimicking strategy	5.09	0.95	0.88	5.80	96	91	-	[50]
Single-atom alloy SACs	Pd-based alloy	PdNi	Template method	-	-	0.95	-	-	-	-20	[51]
		PdAg alloy	Under potentially deposited	-	-	-	-	-	-	-	[52]
		Pd–Ir	The polyol process	-	-	0.626	-	176	-	-	[53]

Table 1 (continued)

Type	Name	Full name	Synthesis method	Loading amount of metal (wt%)	E_{onset} (V)	$E_{1/2}$ (V)	J_L (mA cm^{-2})	Tafel slope (dec^{-1})	Stability Current retention (%)	Shift of reduction potential (mV)	Refs
Double metal SACs	Fe/Ni-N-C	ZIF-8@Fe-Ni	Pyrolysis	-	-	0.91	5.6	81	-	-	[54]
		Fe/Ni-N-C	Pyrolysis	0.25	-	0.86	-	-	-	-20	[55]
		S-FeNi/NiFe$_2$O$_4$@NC	Pyrolysis	10–13	0.96	0.84	-	53	-	-	[56]
		Fe/Ni(1:3)-NG	Hydrothermal reaction strategy	1.19–0.94	-	0.842	-	-	-	-23	[57]
		Fe/Ni-N-C	Pyrolysis	-	0.90	0.81	-	-	-	-	[58]
	Fe/Co-N-C	FeCo-NSC	Pyrolysis	0.37–0.43	-	0.86	5.26	75	86.1	-	[59]
		FeCo-NCps	Micro-mesopore confinement synthetic strategy	0.58–0.27	1.05	0.845	-	90.8	-	-	[60]
		Fe/Co-MWCNT	Pyrolysis	-	0.93	0.86	-	-	82	-	[61]
		Fe/Co-N-C	High-temperature calcination pyrolysis	15–16.8	0.99	0.83	4.33	80	87.5	-	[62]
		Fe/Co-N-C	Pyrolysis	-	0.97	0.86	-	74	-	-	[63]

carbon (Fe-NPC) SACs through a simplified one-pot method (Fig. 5b1), exhibiting an oxygen reduction peak potential of 0.775 V, an E_{onset} of 0.971 V, and a J_L of 6.55 mA cm^{-2} (Fig. 5b2-3).

Furthermore, the inaccessibility of Fe–N–C sites and the low Fe loading are important reasons, which limit the overall ORR activity. To solve the influence of this factor, Han et al. [30] synthesized Fe–N–C (Fig. 5c1) by using KIT-6, Fe(II)-Phen, and 2-methylimidazole, displaying an E_{onset} of 0.93 V and J_L of 8.14 mA cm^{-2} higher than that of Pt/C (0.84 V, 6.57 mA cm^{-2}; Fig. 5c2-3), approximately 93 mV. Cao et al. [31] developed a molten-salt-assisted thermal emitting approach, taking ZIF-8 template to transform bulk ferric(III) oxide powder into a Fe–N–C for ORR (Fig. 5d1). The Fe–N–C presented an $E_{1/2}$ of 0.896 V (Fig. 5d2) and an ORR Tafel slope of 42 mV dec^{-1} (Fig. 5d3). Han et al. [32] synthesized a Fe–N–C by incorporating Fe-Phen complexes into the nanocages during the in situ growth of ZIF-8, followed by pyrolysis at 900 °C under inert atmosphere exhibiting an $E_{1/2}$ of 0.91 V. Chen et al. [33] synthesized Fe–N–C via ultrasonic plasma engineering and direct carbonization in a precursor solution containing metal phthalocyanine and aniline. It exhibited the ORR E_{onset} and $E_{1/2}$ of Fe–N–C equaled 0.92 V and 0.80 V. Moreover, Fe–O–C has attracted extensive attention because it can selectively achieve ORR of 4e by adjusting the metal central atom or non-metallic coordination environment [96]. Guo et al. [34] constructed a graphene-based Fe–O–C via a facile graphene-assisted wet chemical route (Fig. 5e1). Its morphology is shown in Fig. 5e2; the formation of Fe–O–C bond between Fe and graphene can boost 4e path, exhibiting an E_{onset} of 1.00 V (Fig. 5e3) and a good durability (Fig. 5e4).
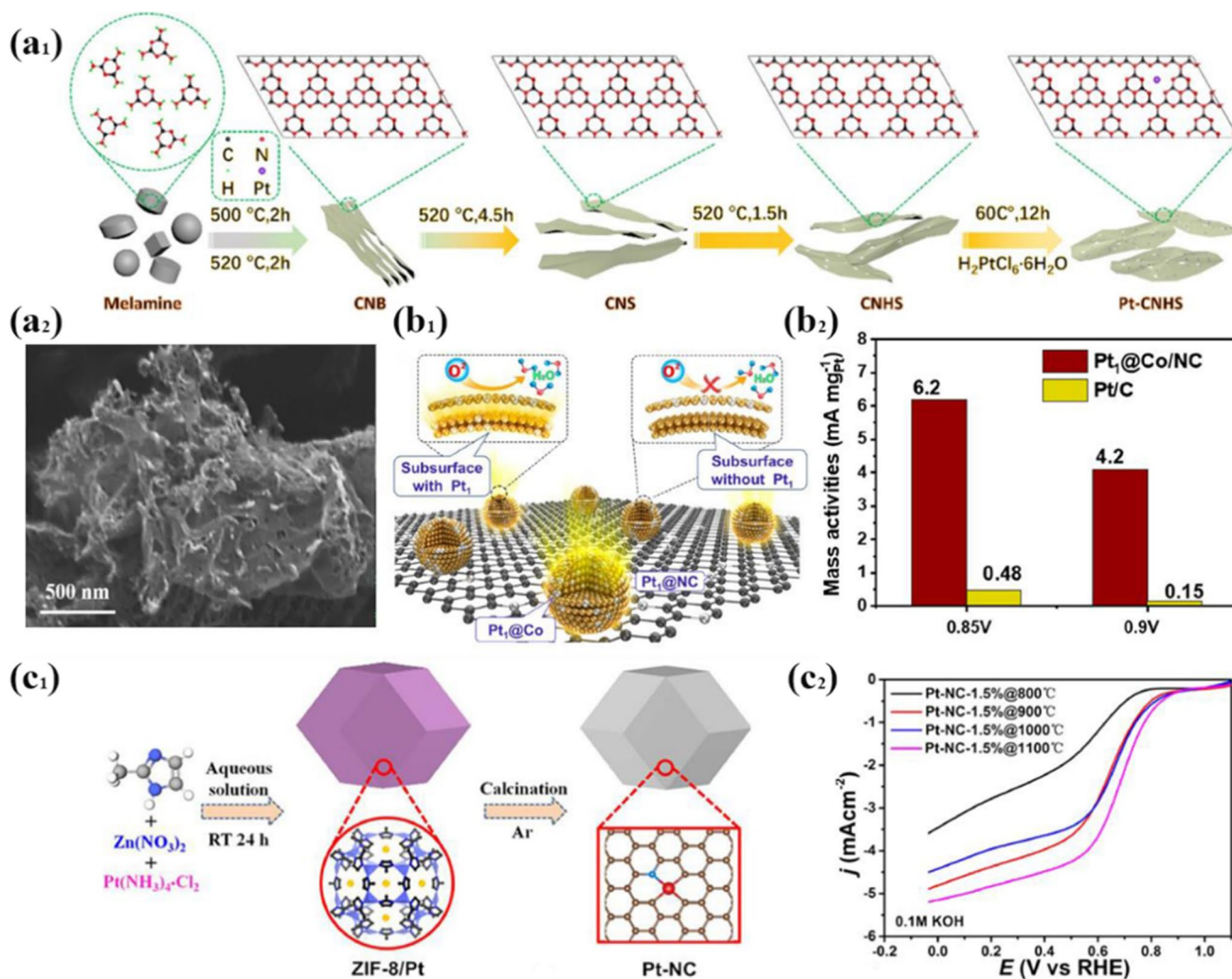
Co–N–C

Due to the inevitable side reaction of Fe-based materials, namely the Fenton reaction, it leads to poor stability and rapid degradation [97]. Therefore, Fe-free catalysts have gradually attracted attention. Co–N–C has attracted extensive exploration due to their high ORR inherent activity and high stability [98–100].

To simplify synthesis steps and improve catalytic performance, Xiong et al. [35] prepared Co–N$_4$–C derived from a *Chlorella* precursor via a straightforward pyrolysis strategy assisted by the high polarization force of a NaCl/KCl eutectic system (Fig. 6a1), exhibiting an E_{onset} of 0.81 V and an $E_{1/2}$ up to 0.83 V (Fig. 6a2-3). Xu et al. [36] synthesized Co–N$_4$–C atomically dispersed in the porous shell via integrating core–shell electrospun. The Co–N–C exhibited superior ORR activity with $E_{1/2}$ of 0.84 V and J_L of 5.22 mA cm^{-2}. Xu et al. [37] synthesized a single Co atom embedded in the sandwich peak porous N-doped double carbon structure (NMCS-rGO-Co; Fig. 6b1-2). The

Table 2 Comparative ORR performance of various SACs in acid solution

Type	Name	Full name	Synthesis method	Loading amount of metal (wt%)	E_{onset} (V)	$E_{1/2}$ (V)	J_L (mA cm^{-2})	Tafel slope (dec^{-1})	Current retention (%)	Shift of reduction potential (mV)	Refs
Noble metal SACs	Pt–N–C	Pt$_1$@Co/NC	ALD	2.2	-	0.863	-	-	-	-	[64]
		Pt–N$_4$–C	Electrostatic adsorption approach	7.13	-	0.886	-	-	-	-112	[65]
	Pd–N–C	C@C$_3$N$_4$–Pt$_1$	Wetness impregnation method	0.5	0.67	-	-	-	-	-	[66]
Transition metal SACs	Fe–N–C	Fe–NPC	One-pot method	-	0.896	-	6.53	-	82	-	[29]
		Fe–N–C/N–OMC	Pyrolysis	2.9	0.91	0.73	5.65	76	-	-	[30]
	Zn–N–C	A–Zn@NSG	Pyrolysis	1.02	0.90	0.85	6.35	39.64	-	-31	[45]
		Zn–N–C	Pyrolysis	9.33	-	0.746	-	-	-	-	[47]
		Zn–B/N–C	Pyrolysis	2.4	-	0.753	-	50	87.6	-	[48]
	Mn–N–C	PT-MnN$_4$	Bio-mimicking strategy	5.09	0.95	0.73	5.80	186	-	-	[50]
Single-atom alloy SACs	Pt based alloy	Pt–Co	Pyrolysis	-	-	0.85	-	82	-	-	[67]
		Pt–Ni	Fluidized bed reactor atomic layer deposition	-	-	-	-	-	-	-	[68]
Double metal SACs	Pt/Ni–N–C	Pt$_{0.7}$Ni$_{0.3}$/C	Low-temperature impregnation-reduction method	10	-	0.811	5.39	69.52	90.4	-	[69]
		Pt–Ni PND	ALD	-	-	0.930	-	-	75	-	[70]
	Fe/Ni–N–C	Fe/Ni–N–C	Pyrolysis	0.25	-	0.86	-	-	100	-	[55]

Fig. 3 a_1 Illustration of the CNHS and Pt-CNHS; a_2 FESEM images of Pt-CNHS [25]. Copyright 2021, Elsevier. b_1 The structure of Pt@Co/NC with and without Pt, b_2 compared to the mass activities of Pt@Co/NC and Pt/C [64]. Copyright 2021, American Chemical Soci- ety. c_1 Schematic of fabricating Pt–N–C; c_2 linear sweep voltamme- try (LSV) curves of Pt–NC–1.5% samples under different calcination temperatures [26]. Copyright 2021, Elsevier.

Co–N–C exhibited an $E_{1/2}$ of 0.72 V (Fig. 6b3). Yang et al. [38] proposed a catalyst consisting of high-purity pyrrole N anchored Co single-atom (CoN4). The Co–N–C exhibited an $E_{1/2}$ of 0.84 V at 10 mA cm^{-2}.

Ni–N–C

Ni–N–C has been considered promising catalyst for various bat- teries because of good dynamics, high conductivity, and chemical stability. The local environment of single atom is sensitive to the supports, location, and surrounding heteroatoms. Such as a boosted ORR is achieved with the decrement in coordinated Ni atoms for Ni–N–C. Inspired by this, Luo et al. [39] regulated the coordination of Ni–N–C by a secondary single-atom modulation strategy (Fig. 7a1). The obtained Ni–N–C displayed an $E_{1/2}$ of

0.854 V ((Fig. 7a2). Qiu et al. [40] developed Ni–N–C with a loading of ≈ 23 wt% by the chemical vapor deposition (CVD) process and chemical etching (Fig. 7b1). The Ni–N–C exhib- ited an E_{onset} of 0.984 V, an $E_{1/2}$ of 0.859 V ((Fig. 7b2). Zhao et al. [41] synthesized Ni–N–C supported on N-doped carbon nanotube (Ni–N-CNT) with a loading of 20.3 wt% via a one-pot pyrolysis method by employing Ni acetylacetonate and dicyan- diamide precursors (Fig. 7c1). The Ni–N–C exhibited an E_{onset} of 0.88 V and an $E_{1/2}$ of 0.75 V (Fig. 7c1).

Cu–N–C

Cu–N–C is commonly used SACs with catalytic proper- ties due to hydrogenation, dehydrogenation, and oxidation [101]. Significantly, the ORR inherent of Cu–N–C is com- pared to Pt/C and the method of synthesizing catalyst is
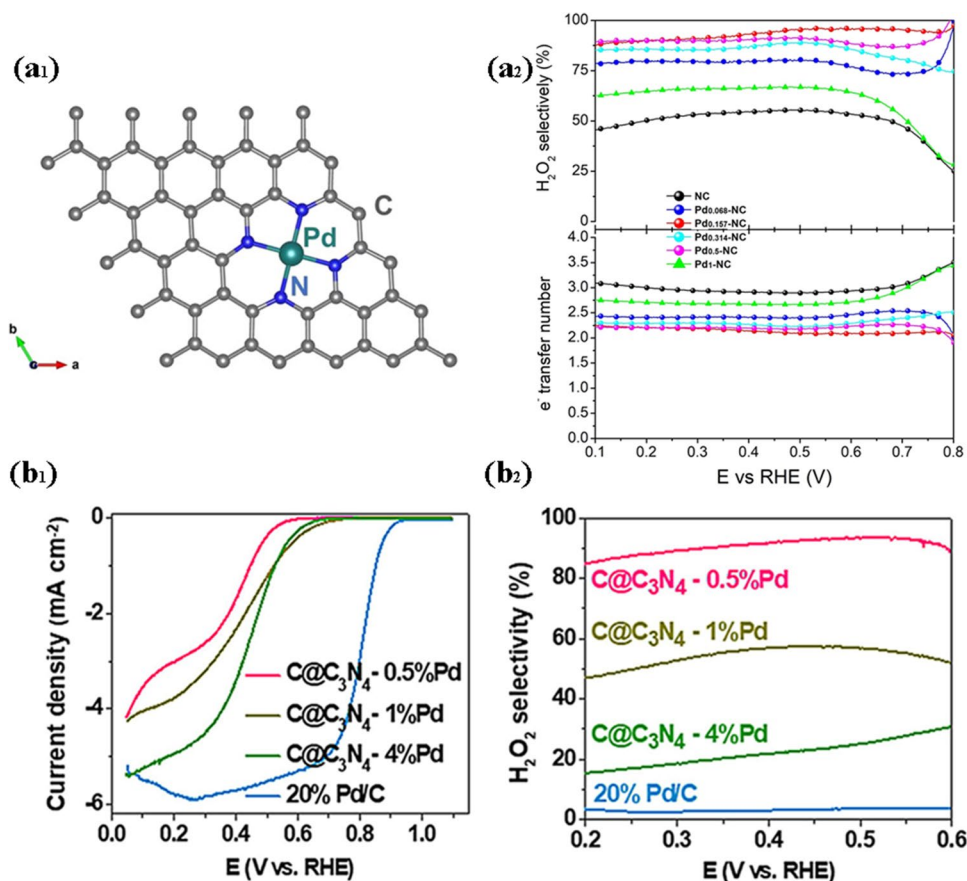
facile. Thus, this novel catalyst is a promising alternative ORR replacing Co/C catalyst.

For improving ORR of Cu–N–C catalysts, Ji et al. [42] fabricated Cu–N–C by using 2,6-diaminopyridine C/N source and silica template (Fig. 8a1). The Cu–N–C delivered high ORR activity with an $E_{1/2}$ of 0.83 V and a J_L of 5.25 mA cm^{-2} (Fig. 8a2). Combination with Cu and polymer is also a method to improve the ORR performance. Ma et al. [43] fabricated Cu–N–C with the designed coordination structure by an ionic exchange strategy. The obtained Cu–N–C-900 exhibited an $E_{1/2}$ of 0.87 V and Tafel slope of 79 mV dec^{-1} (Fig. 8b1–2). Han et al. [44] reported the single-atom Cu supported on graphene with a loading of 5.4 wt% by a confined self-initiated dispersing protocol (Cu/G; Fig. 8c1). The $E_{1/2}$ and J_L of the optimized Cu–N–C were 0.85 V and 3.787 mA cm^{-2}, respectively (Fig. 8a2).

Zn–N–C

Due to the high volatility of metal Zn, Zn-based materials have less progress for the transition metal catalysts [102, 103]. But, the Zn-based precursors are applied in producing porosity via pyrolysis for the Zn-free SACs [104–107]. Moreover,

Zn–N–C catalysts were active for various electrochemical reactions.

Jiang et al. [45] reported the catalyst with Zn sites supported on N and S co-doped biomass graphene (A-Zn@NSG; Fig. 9a1). The Zn–N–C exhibited an $E_{1/2}$ of 0.805 V in 0.1 M HClO$_4$ and 0.905 V in 0.1 M KOH (Fig. 9a2-3). Wang et al. [46] synthesized single Zn atoms dispersed on N-doped hierarchically porous carbon (Zn–N–C) by employing apples, egg whites, and ZnCl$_2$ raw materials (Fig. 9b1–2). The catalyst exhibited an $E_{onset} = 0.85$ V, $E_{1/2} = 0.78$ V, and $J_L = 4.71$ mA cm^{-2} in 0.1 M KOH electrolyte solution (Fig. 9b3-4).

Owing to the high volatility of the metal Zn at high temperature, the Zn loading in Zn–N–C catalysts still remains a formidable challenge [108, 109]. Li et al. [47] prepared a Zn–N–C catalyst with a Zn loading of 9.33 wt% by adopting a low annealing rate of 1 °C min^{-1}. The Zn–N–C catalyst largely maintained its Zn–N$_x$ active sites, and the $E_{1/2}$ decayed by only 19.88 mV after 1000 CV cycles. Wang et al. [48] synthesized Zn–N–C catalyst via a facial one-step strategy, giving a Zn loading of 2.4 wt% (Fig. 9c1). The Zn–N–C showed an $E_{1/2}$ of 0.886 V and an average number of 4.08 (Fig. 9c2-3).
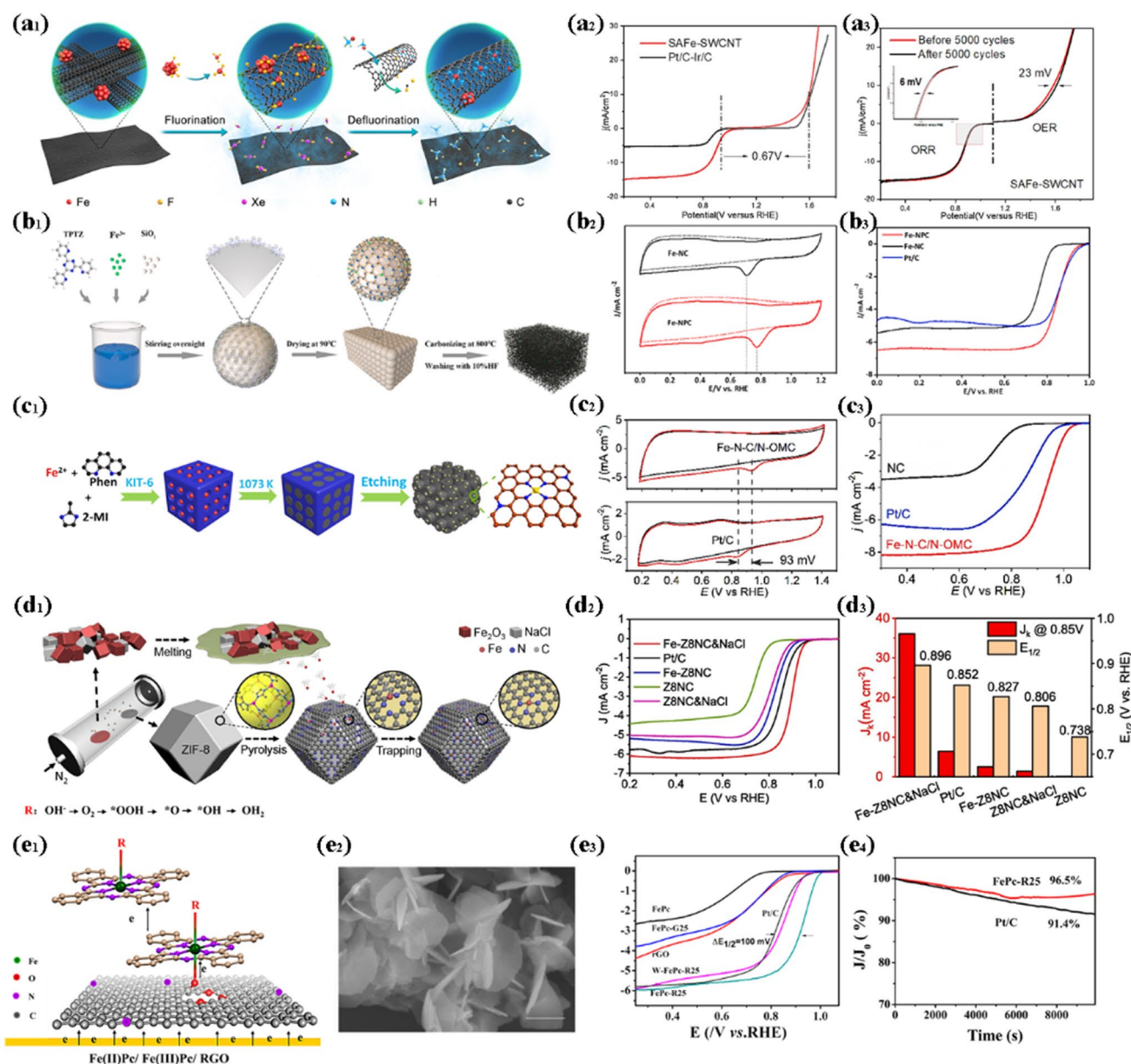
Fig. 5 a_1 Schematic of the SAFe-SWCNT; a_2, a_3 electrocatalytic performance of the SAFe-SWCNT and Pt/C-Ir/C [28]. Copyright 2021, Elsevier. b_1 The diagram of Fe-NPC sample; b_2 CV curves and b_3 LSV curves of the samples [29]. Copyright 2022, Elsevier. c_1 Illustration of Fe–N–C/N-OMC catalyst; c_2 CV curves and ORR; c_3 LSV of the samples in 0.1 M KOH electrolyte [30]. Copyright 2021, Else-vier. d_1 Schematic of the Fe-ZIF-8NC and NaCl based on the salt-assisted emitting approach; d_2 the corrected LSV at 1600 rpm; d_3 $E_{1/2}$ and current density at 0.85 V [31]. Copyright 2021, Elsevier. e_1 The structure and ORR mechanism of Fe–O–C; e_2 SEM: e_3 LSV curves of Fe–O–C; e_4 chronoamperometric test curves of Fe–O–C [34]. Copyright 2018, Elsevier.

## Mn–N–C

Mn–N–C is used SACs with high potential due to cheap, non-toxic, and widely sourced [110, 111]. Mn considered as an active metal for ORR electrocatalysis compared to zirconium [112, 113].

Mn–N–C is generally low active for the ORR under alkaline conditions. To solve this problem, Lin et al. [49] synthesized the Mn–N–C supported on the carbon frame-works (Fig. 10a1), displaying an $E_{1/2}$ of 0.87 V (Fig. 10a2). Inspired by the catalytic activity and selectivity of enzymes, Yan et al. [50] designed ultrathin carbon nanosheet-supported Mn–N$_4$–C (PT-MnN$_4$) by using a bio-mimicking strategy (Fig. 10b1). The Mn–N–C showed an E_{onset} of 0.95 V, an $E_{1/2}$ of 0.88 V, and a J_L of 5.80 mA cm^{-2} (Fig. 10b2-3).

Fig. 6 a_1 The preparation scheme for Co–N/C-SAC; a_2 CV and a_3 LSV of the samples [35]. Copyright 2021, Elsevier. b_1 Illustration of NMCS-rGO-Co; b_2 TEM images for the NMCS-rGO-Co; b_3 LSV curves [37]. Copyright 2022, Elsevier.
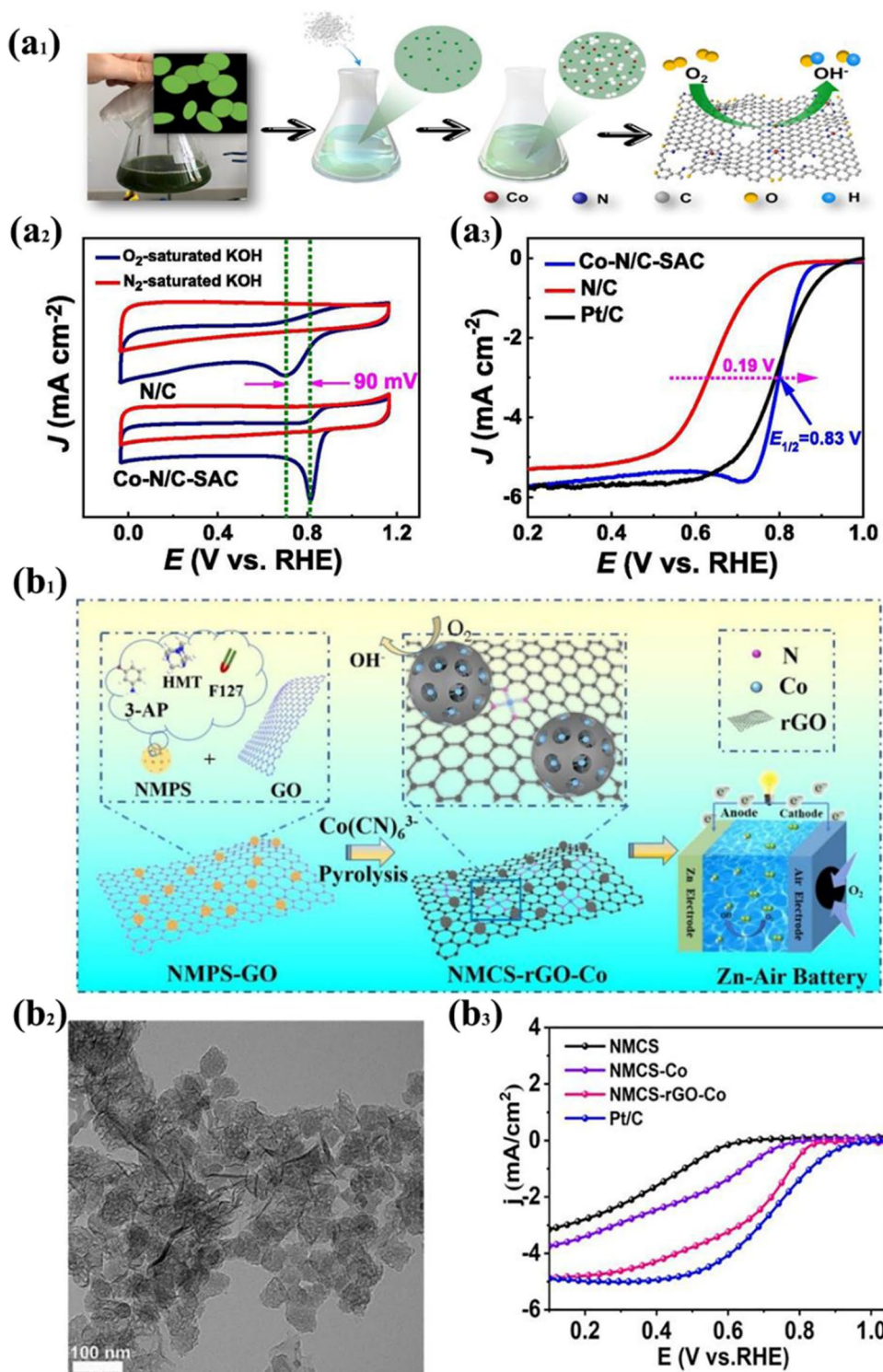
Others

Other transition metals can also have ORR perfor-
mance. As a case, Liu et al. [114] reported Sn–N–C
with an $E_{1/2}$ of 0.87 V and excellent durability. Luo
et al. [115] used a metal–organic framework as an
anchoring matrix obtained pyrolyzed Cr–N–C. It
exhibited an $E_{1/2}$ of 0.773 V and showed superb sta-
bility. Xue et al. [116] reported a Mo–N–C exhibiting
excellent activity and selectivity toward electrochemi-
cal reduction reaction with favorable limiting potential
of 0.40 V.
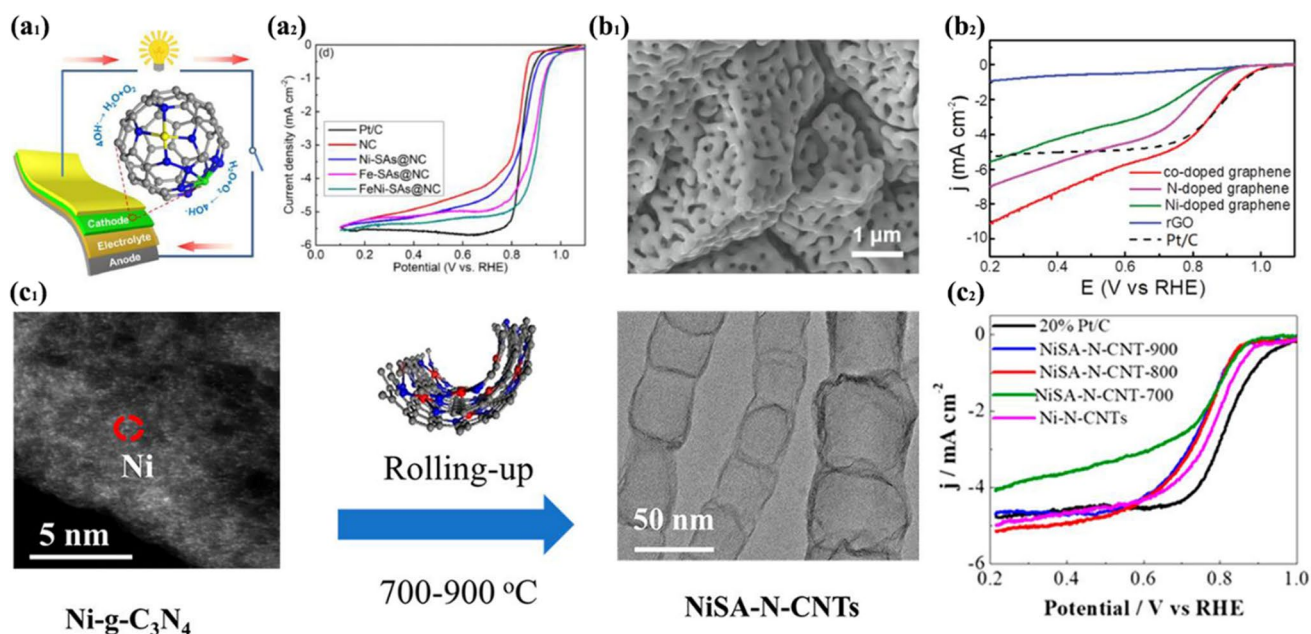
Fig. 7 **a**$_1$ Scheme of the all-solid-sate ZABs; **a**$_2$ LSV curves of the samples [39]. Copyright 2021, Elsevier. **b**$_1$ SEM images of N-doped graphene/porous Ni; **b**$_2$ ORR LSV of different samples [40]. Copy-right 2019, Wiley. **c**$_1$ Diagram of the forming procedures for Ni SAC; **c**$_2$ the ORR curves on Ni–N-CNT SAC electrocatalysts [41]. Copyright 2018, American Chemical Society.

Single-atom alloy SACs

Single-atom alloys with the characteristics of unique electronic structures and well-defined active sites demonstrated the promising potential to replace traditional metal catalysts [117]. The advantages of decoupling the dissociation and reaction sites in electrocatalysis are expected to tailor the adsorption properties of reaction species, thus promoting electrocatalytic behaviors [118]. We discussed the progress of Pt–M (Pd, Co, Ni) and Pd–M (Ag, Ir, Co, Ni) in this section (Tables 1 and 2).

Pt–M (Pd, Co, Ni)

To diminish the Pt loading, manufacturing Pt-based alloy catalysts (Pt–M) has made great progress, wherein M can tailor the electronic and geometric structures to improve the ORR activity [119]. Zhang et al. [120] synthesized Pt–Pd SACs on nitrogen-doped carbon nanotubes by ALD technology (Fig. 11a1). The catalyst showed a mass activity of 0.91 mA g_{Pt}^{-1} and good durability (Fig. 11a2). Cheng et al. [67] reported a Pt–Co SAC by pyrolysis method (Fig. 11b1). The catalysts exhibited an $E_{1/2}$ of 0.85 V (Fig. 11b2) and Tafel slope of 82 mV dec^{-1} in 0.1 M HClO$_4$ solution. Lee et al. [68] presented a strategy of active Pt–Ni SACs via fluidized bed reactor ALD (FBR-ALD; Fig. 11c1). The catalyst exhibited a mass activity of 0.57 mA $μg_{Pt}^{-1}$ (Fig. 11c2).

Pd–M (Ag, Ir, Co, Ni)

Pd-based alloy catalysts have been regarded as potential substitutes for Pt catalysts. Both Pd and Pt are platinum group metals adjacent in the periodic table and share similar electronic structures and properties. However, Pd is more cost-effective than Pt [121]. For a case, Betancourt et al. [52] synthesized Pd–Ag alloy catalyst by using under potentially deposited (UPD; Fig. 12a1). With Pd modifying Ag/C, the ORR $E_{1/2}$ was shifted to more positive values, and the overpotential is significantly reduced along with an overall activity increment observed as an increase in Pd (Fig. 12a2). Kim et al. [53] prepared a Pd–Ir alloy catalyst via the polyol process. The $E_{1/2}$ of catalysts can reach 0.626 V (Fig. 12b1), and Tafel slop can reach 176 V dec^{-1} (Fig. 12b2). Wei et al. [122] reported that the metal only grows and spreads out in two dimensions, the freestanding and self-stabilized Pd–Co SAL generated in the angstrom-sized interlayer space of layered minerals (Fig. 12c1). Pd–Co SAL presented a good ORR performance (Fig. 12c2) and a mass activity of 0.257 mA $μg_{Pd}^{-1}$ (Fig. 12c3). Sahoo et al. [51] reported an ultrathin twisty Pd–Ni alloy catalyst (Fig. 12d1). The catalysts exhibited a low reaction overpotential with an $E_{1/2}=0.95$ V (Fig. 12d1).

Others

Noble metal-free alloy catalysts have always been a research hotpot due to the rich resources. However, it is still a challenging to develop noble metal-free alloy catalysts. Nam et al. [123] synthesized a Cu–Fe alloy SACs, exhibiting a
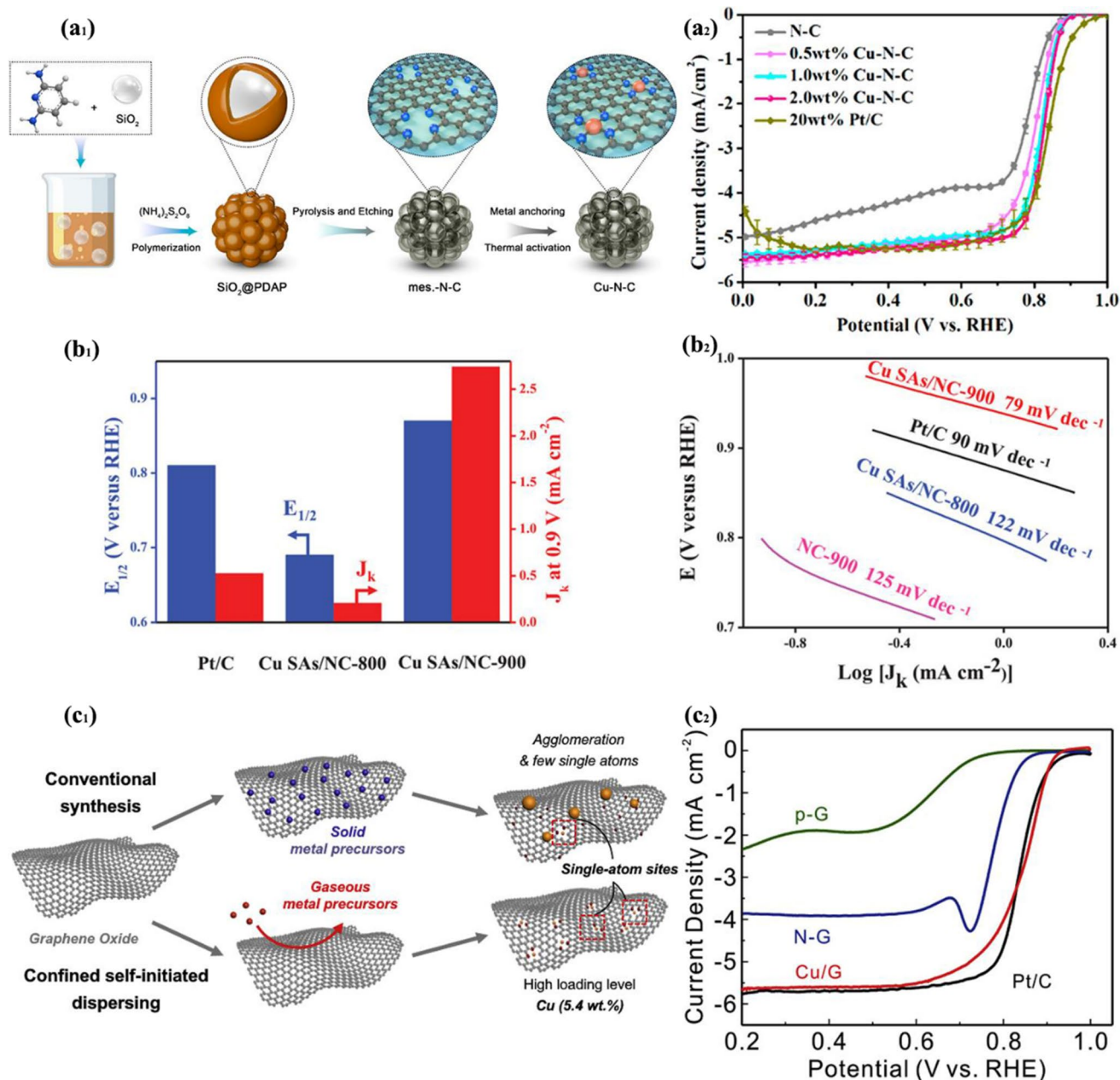
Fig. 8 a_1 Illustration of the Cu–N–C; a_2 ORR LSV of Cu–N–C samples [42]. Copyright 2021, American Chemical Society. b_1 $E_{1/2}$ and current density of Cu–N–C and Pt/C; b_2 Tafel plots of the samples [43]. Copyright 2020, Wiley. c_1 Schematic conventional and confined self-initiated dispersing protocols; c_2 ORR LSV of the samples [44]. Copyright 2019, Elsevier.

good ORR activity compared to that of Pt–C electrocatalysts. Niu et al. [124] reported Co–Ni alloy catalyst synthesized from metal precursors and dicyandiamide nanofibers formed by freeze-drying pretreatment. The catalyst exhibited an E_{onset} of 0.9 V, an $E_{1/2}$ of 0.84 V, and a J_L of 6.4 mA cm^{-2}.

Double metal SACs

For solving the defects of SACs, multiple atomic active sites and high metal loading have been gradually designed and constructed in recent years [125–127]. Double-metal SACs (DMSACs) were born. Recent research proved that the SAC activity can be enhanced by adding a second metal atom, pointing out the research direction of DMSACs [128]. DMSACs composed of bonded two metal atoms and coordination of metal pairs with N atoms in carbon framework, opposite to M–N–C SACs. Such configuration could improve the electrocatalytic activities of metal centers (Tables 1 and 2) [129, 130].
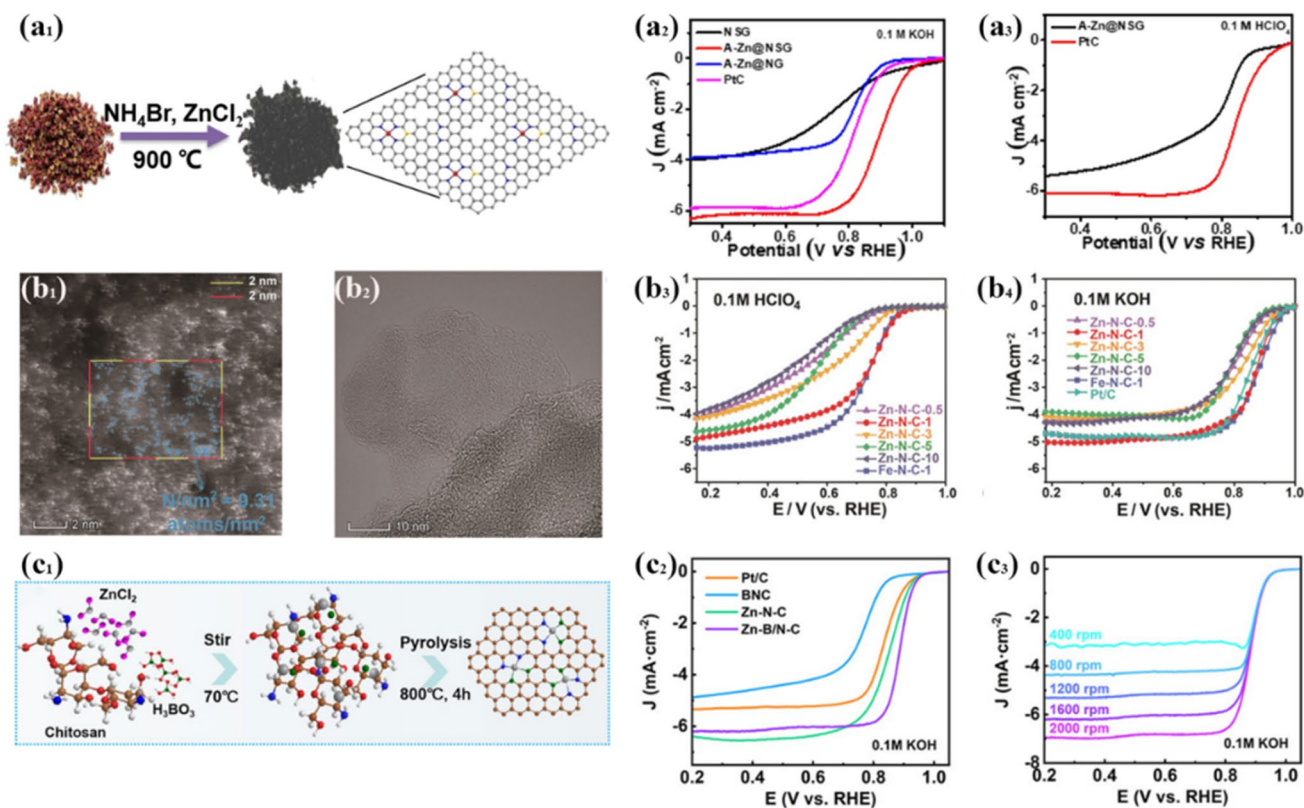
Fig. 9 a_1 Preparation diagram of A-Zn@NSG; a_2 LSV curves for A-Zn@NSG, A-Zn@NG, NSG, and Pt/C (20%); a_3 LSV curves of A-Zn@NSG and Pt/C (20%) [45]. Copyright 2021, American Chemical Society. b_1 HAADF-STEM image of Zn–N–C; b_2 HRTEM image of Zn–N–C; ORR LSV of Zn–N–C–X and Fe–N–C–X catalysts recorded in O_2-saturated 0.1 m KOH b_3 and 0.1 m HClO$_4$ solution b_4 [46]. Copyright 2019, Wiley. c_1 Diagram for the Zn–B/N–C synthesis; c_2 LSV curves of different samples; c_3 LSV curves at different rotation rates [48]. Copyright 2020, Wiley.

Pt/Ni–N–C

Although Pt-SAC has some advantages, the shortage of resources reduces the commercial value of Pt [131]. Therefore, researchers began to adopt a diatomic approach, aiming to reduce the content of Pt while maintaining or increase its ORR performance. Pt/Ni–N–C is a promising ORR catalyst due to that the alloying Pt with Ni can reduce the Pt content and increase its intrinsic activity [132]. Liu et al. [69] designed Pt/Ni–N–C by using a low-temperature impregnation–reduction method (Fig. 13a1), exhibiting more satisfactory ORR performance, a remarkable cathodic peak (Fig. 13a2), more positive $E_{1/2}$, and incremental J_L (Fig. 13a3). Wan et al. [133] prepared a Pt/Ni–N–C showing a high mass activity of 3.25 ± 0.14 mA μgPt^{-1} at 0.9 V. Li et al. [70] synthesized a Pt/Ni–N–C with a nanoflower structure by controlling the surface-active agents (Fig. 13b1), exhibiting the $E_{1/2}$ of 0.930 V (Fig. 13b2-3).

Fe/Ni–N–C

Both Fe and Ni elements are ideal SACs, which have excellent electrocatalytic performance [134]. With the rise of DMSACs, the preparation of DMSACs with high ORR performance by combining Fe and Ni and anchoring on the same matrix has attracted the interest of researchers [135].

Bai et al. [54] reported a host–guest method to load the Fe–Ni-mIm (guest) on the surface of ZIF-8 (host), and the resulting ZIF-8@Fe–Ni(mIm)X precursors can be converted to Fe/Ni–N–C after carbonization (Fig. 14a1). The Fe/Ni–N–C exhibited an $E_{1/2} = 0.91$ V and a loss of 6 mV after 5000 cycles (Fig. 14a2-3). Liu et al. [55] synthesized a dual metal (Fe, Ni)-N-doped carbon (Fe/Ni–N–C) by the pyrolysis of Fe, Ni co-doped ZIF-8 exhibiting the $E_{1/2}$ of 0.79 V in HClO$_4$ and 0.86 V in NaOH electrolyte. Wang et al. [56] presented an elaborate method for preparing Fe/Ni–N–C in N-doped carbon via introducing Fe/Ni Hofmann-type MOFs precursors. As-obtained Fe/Ni–N–C showed an ORR potential gap of 0.76 V.
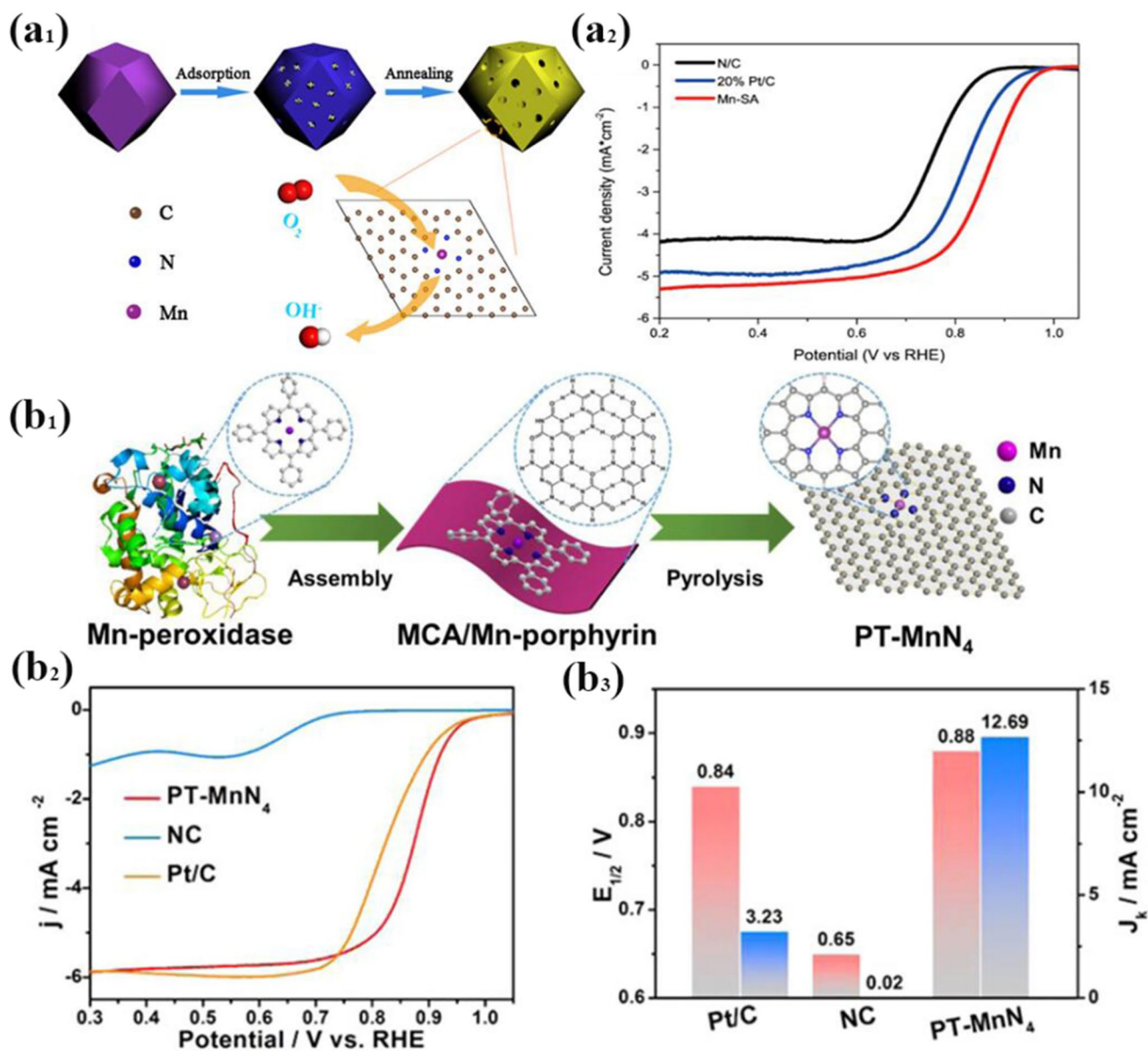
Fig. 10 $\mathbf{a_1}$ The synthesis route of the Mn–N–C; $\mathbf{a_2}$ LSV curves of the Mn–N–C SAC, N/C, and 20 wt% Pt/C [49]. Copyright 2020, American Chemical Society. $\mathbf{b_1}$ Illustration of pyrrole-type (PT)-MnN$_4$; $\mathbf{b_2}$ LSV curves of PT-MnN$_4$, NC, and Pt/C; $\mathbf{b_3}$ $E_{1/2}$ and kinetic current density of PT-MnN$_4$, NC, and Pt/C [50]. Copyright 2021, Wiley.

In addition, graphene is also a popular material for electrocatalysis [136]. To anchor metal ions by the trapping ability of graphene, Ma et al. [57] synthetized the Fe/Ni–N–C supported on the N-doped graphene (Fe/Ni(1:3)-NG; Fig. 14b1), exhibiting good ORR performance and excellent stability ($E_{1/2}=0.842$ V; Fig. 14b2-3). Sirirak et al. [137] synthesized Fe/Ni–N–C (Fe/Ni-NG) supported on graphite oxide via thermal annealing of GO-mixed melamine under N$_2$ atmosphere. The E_{onset} for Fe/Ni-NG is 0.61 mV positive shift compared with NG alone (0.48 V). Its peak potential is 0.12–0.34 V. Zhang et al. [58] reported a novel oxygen electrode catalyst based on bimetal Fe–Ni atoms anchored on N-doped graphene-like carbon (Fe/

Ni–N–C). The ORR E_{onset} and $E_{1/2}$ of Fe/Ni–N–C were about 0.90 V and 0.81 V.

Fe/Co–N–C

It has been found that Fe/Co–N–C showed tremendous promise for ORR to replace noble metal catalysts due to stability and catalytic activity [138].

Wu et al. [59] synthesized a Fe/Co–N–C in that Fe and Co atoms are stabilized separately on 2D carbon nanosheets via coordination with N and S heteroatoms to form a Fe/Co–N–C.
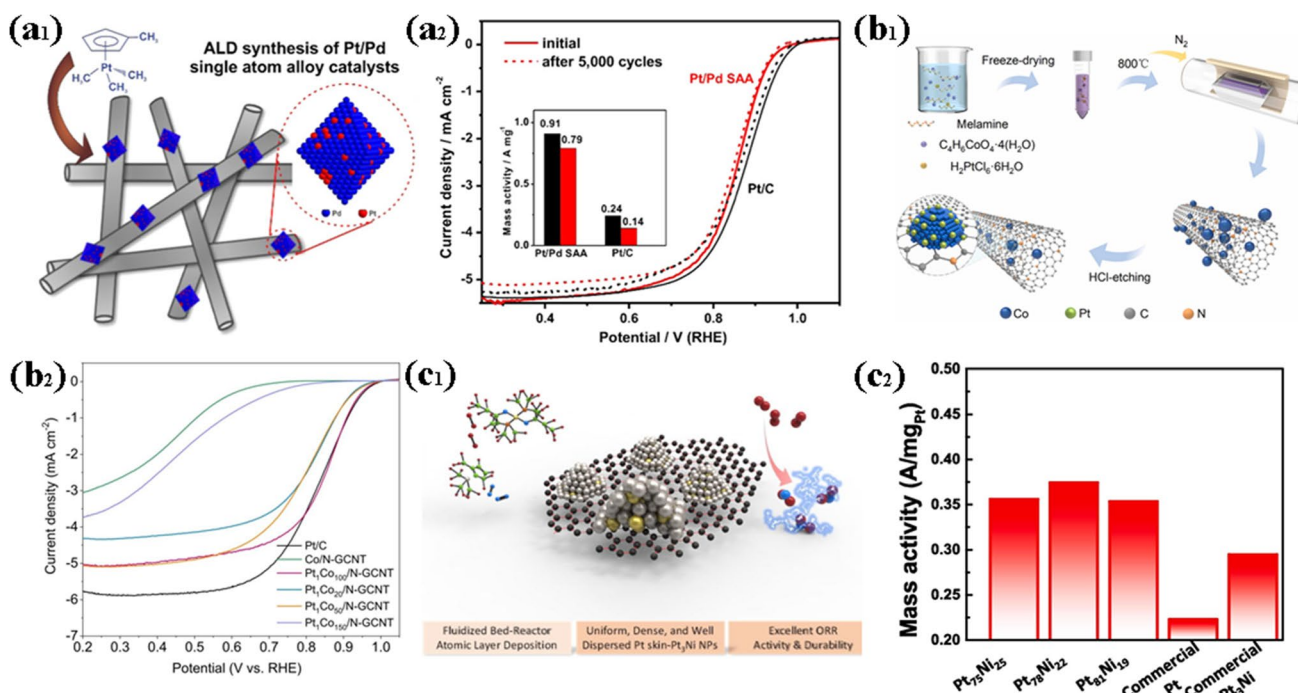
Fig. 11 **a₁** The schematic for the synthetic of Pd–Pd SACs; **a₂** LSV curves of the octahedral Pt/Pd SACs and durability test [120]. Copyright 2019, American Chemical Society. **b₁** The schematic for the synthetic of Pt₁Con/N-GCNT; **b₂** LSV curves [67]. Copyright 2022, Elsevier. **c₁** Schematic of Pd–Ni SACs; **c₂** mass activity of alloy catalysts [68]. Copyright 2022, Elsevier.

The Fe/Co–N–C exhibited outstanding electrocatalytic activities of ORR with an $E_{1/2}$ of 0.86 V, outperforming the Fe and Co SACs. Liu et al. [60] synthesized Fe/Co–N–C via the micromesopore confinement synthetic strategy. The catalyst had superhigh specific surface area and abundant defective structure and displayed excellent ORR performance in 0.1 M KOH ($E_{onset}=1.05$ V, $E_{1/2}=0.845$ V). Kumar et al. [61] prepared Fe/Co–N–C on phthalocyanine-modified multiwalled carbon nanotubes (MWCNTs). The Fe/Co–N–C exhibited an E_{onset} of 0.93 V and an $E_{1/2}$ of 0.86 V (Fig. 15a1-2). Yu et al. [62] via high-temperature calcination pyrolysis of Zn and Co dual-metal sites of ZIF-coated electrospun polyacrylonitrile fibers synthesized the Fe, Co, and N co-doped catalyst (Fe/Co–N–C), exhibiting an E_{onset} of 0.99 V and an $E_{1/2}$ of 0.83 V in 0.1 M KOH solution. Zhou et al. [63] synthesized an efficient Fe/Co–N–C based on N-doped carbon by pyrolysis of Fe/Co and 10-phenanthroline complexes (Fe/Co-phen) supported on ZIF-8 (Fig. 15b1). The Fe/Co–N–C exhibited an E_{onset} of 0.97 V, an $E_{1/2}$ of 0.86 V, and a Tafel slope of 74 mV dec^{-1} (Fig. 15b2-3).

Others

With the deepening of the research on DMSACs, more and more elements are introduced [139]. As a case, Parkash et al. [140] used CTAB reduction method to prepare carrier-free, ultralow Pt content nanostructured Pt/Cu atoms (NPS) with different Pt contents. The Pt/Cu–N–C

exhibited an $E_{onset}=0.98$ V. Xu et al. [141] reported Fe/Zn–N–C supported on porous N-doped carbon frameworks. It achieved an $E_{1/2}$ of 0.78 V, 0.85 V, and 0.72 V in 0.1 M HClO₄, 0.1 M KOH, and 0.1 M phosphate buffer saline solutions, respectively. Gharibiab et al. [142] synthesized Cu/Fe–N–C with an E_{onset} of 0.86 V and a J_L of 6.34 mA cm^{-2} in 0.1 M HClO₄.

Synthetic strategies

The method of accurately preparing SACs is expanding [143, 144]. But when the metal particles are reduced to the single-atom level, the specific surface area and surface free energy will increase sharply, making it easy for single atoms to form large clusters through coupling in the process of preparation and reaction, resulting in reduced catalytic activity [145, 146]. Therefore, the synthesis of SACs remains a huge challenge. In this section, we summarized several synthesis methods and discussed their advantages and disadvantages [147].

Wet chemistry

As a kind of common methods for catalyst preparations, wet chemistry includes impregnation, co-precipitation, and solvothermal method [148]. The wet chemistry methods were

Fig. 12 **a₁** The schematic for Pd–Ag alloy catalysts; **a₂** LSV curves [52]. Copyright 2020, American Chemical Society. **b₁** I–V curves for the ORR activity and **b₂** Tafel slope of Pd–Ir-based ternary alloy catalysts [53]. Copyright 2022, Elsevier. **c₁** Scheme for Pd–Co alloy; **c₂** LSV and **c₃** specific mass activities [122]. Copyright 2022, Elsevier. **d₁** Schematic of Pd–Ni alloy; **d₂** LSV curves of Pd–Ni alloy [51]. Copyright 2022, American Chemical Society.
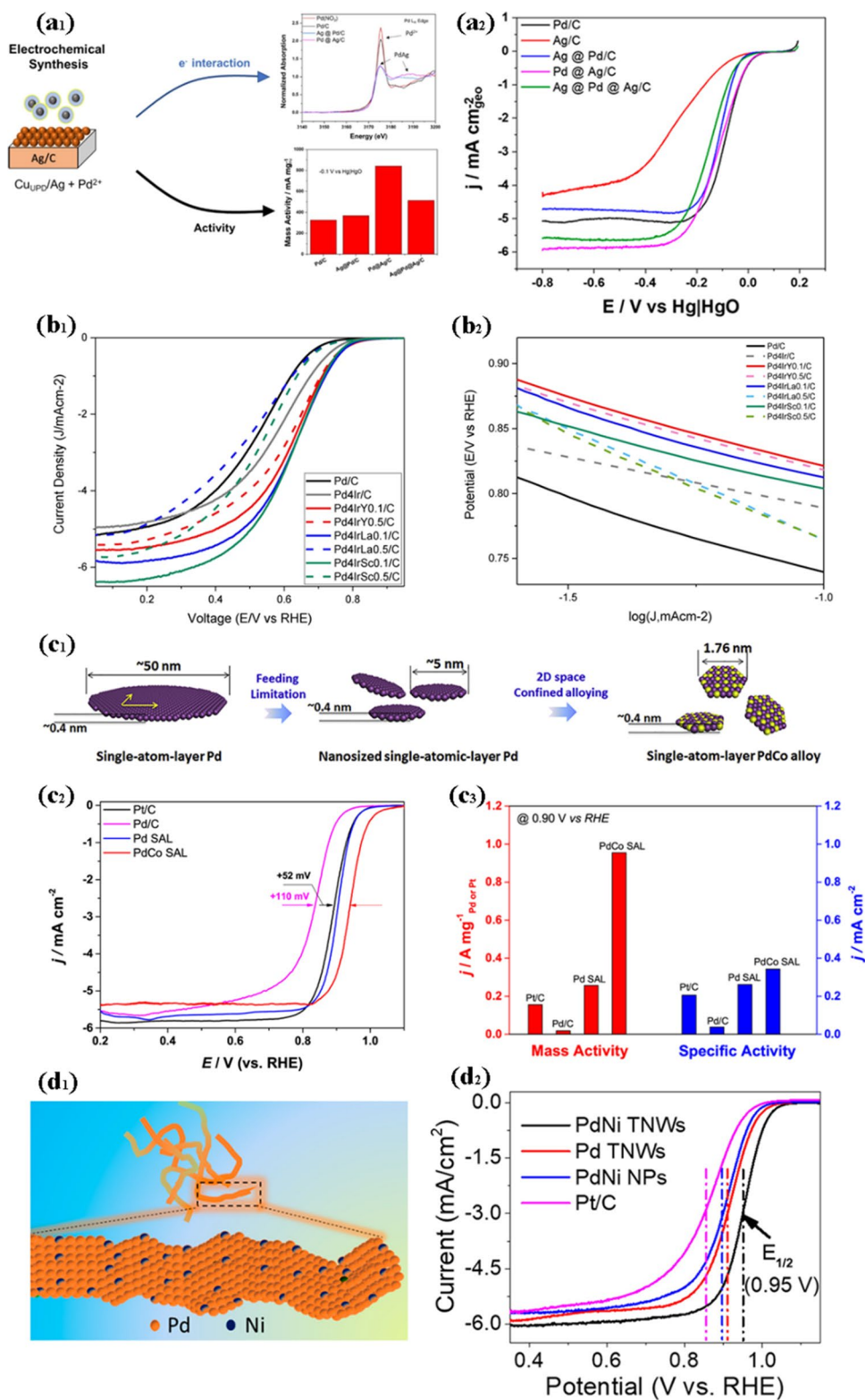

used to prepared SACs by adsorbing metallic ionics in solution and then attaching atoms on the supports. Such methods are employed to synthesize SACs via adjusting the metal selecting and loading [149]. It aims to stabilize the atom species on a suitable supporter via chemical coordination, inhibiting aggregation during the preparation process [150].

Zhang et al. [151] employed an impregnation method to prepare the Pd SACs. Because the interaction between

Fig. 13 a_1 Illustration of PtM NCs (M = Fe, Co, Ni); a_2 CV curves and a_3 ORR LSV of PtM/Cs [69]. Copyright 2019, American Chemical Society. b_1 Diagram of the Pt–Ni PND; b_2 CV curves and b_3 ORR LSV of Pt–Co GND, Pt–Ni PND, and Pt/C [70]. Copyright 2021, Elsevier.
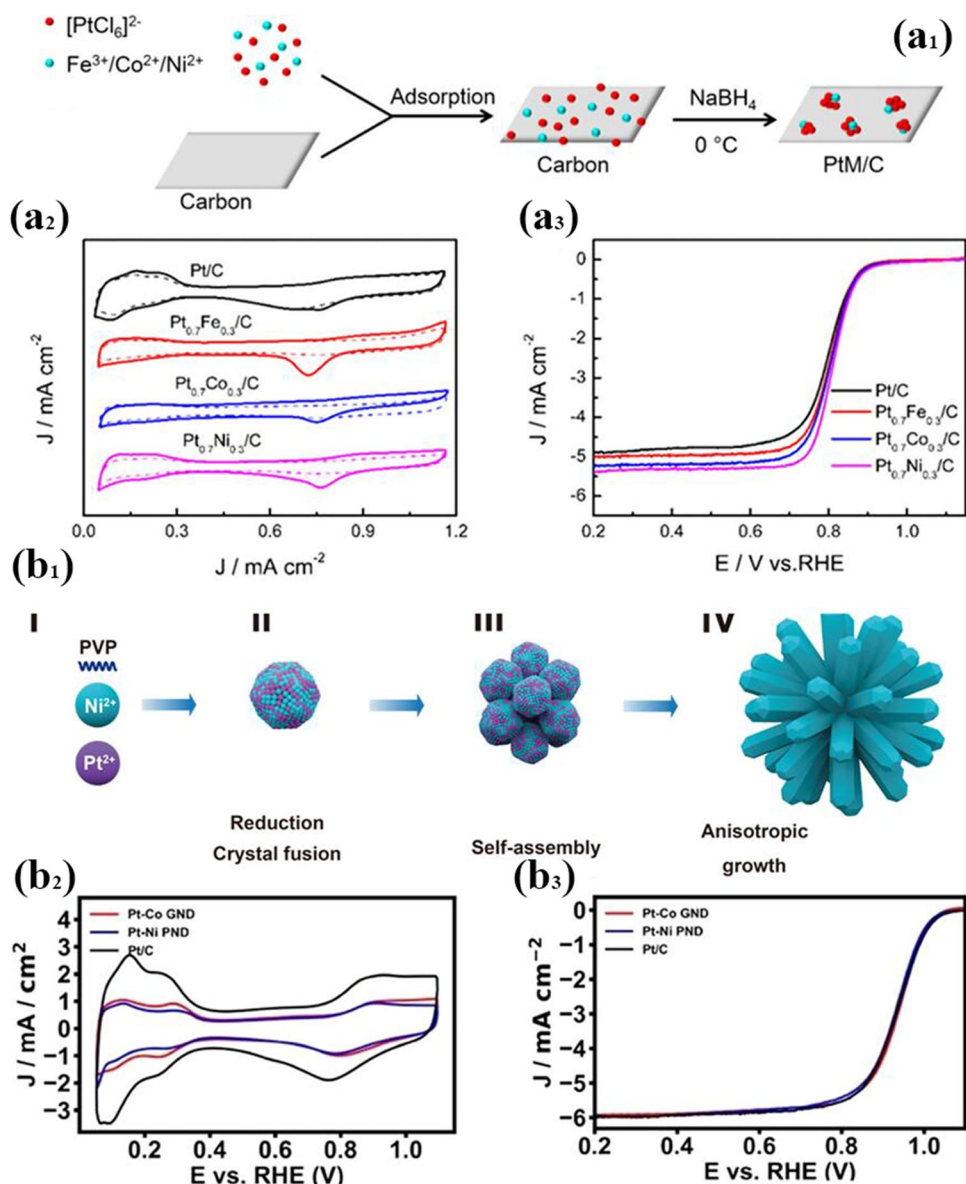

defect sites and functional groups, the Pd^{2+} ions accumulated around the defect sites on the carbon surface of the Pd precursor solutions (Fig. 16a). It improved the in-plane and inter-lamellar separation/transfer of the carrier, improving the ORR efficiency. Zou et al. [152] synthesized ethylenediaminetetraacetic acid-M/CeO_2 catalysts (EDTA, M = Ni or Co, CCI; Fig. 16b1) via a chelation coupled wetness impregnation. The catalysts possess rich oxygen vacancies and interfacial metal active sites (Fig. 16b3). Yi et al. [153] employed the co-precipitation method with Pd^{2+} ions and an ionic liquid of ReO_4^- salt to load single-atom Pt on NBF-ReS_2, realizing high Pd atom utilization efficiency. Qin et al. [154] synthesized Au_x–$NiMn_2O_4$ by a modified solvothermal method (Fig. 16c1). The result showed that the Au atoms dispersed on $NiMn_2O_4$ lattice and occupied the position of Mn, Ni, or O (Fig. 16c2-3), which improved

the electrocatalytic performance of ORR. Lu et al. [155] fabricated Co-MOF SACs based on Co^{2+} source and trimeric acid (H_3BTC) through a solvothermal method (Fig. 16d). More catalytic active sites were provided for high ORR performance.

Wet chemistry has the following advantages. (1) The loading components are only loaded on the surface of the carrier in most cases, which can effectively improve the utilization rate of atoms and reduce the dosage [156]. Therefore, this method is of great significance for Pt-based and other noble metal catalysts and can effectively reduce the amount of noble metals. (2) Different supports can be selected to provide the required physical properties for the catalyst, such as specific surface and pore radius [157]. Therefore, wet impregnation method is a simple and convenient method. Although wet impregnation has the above advantages, there
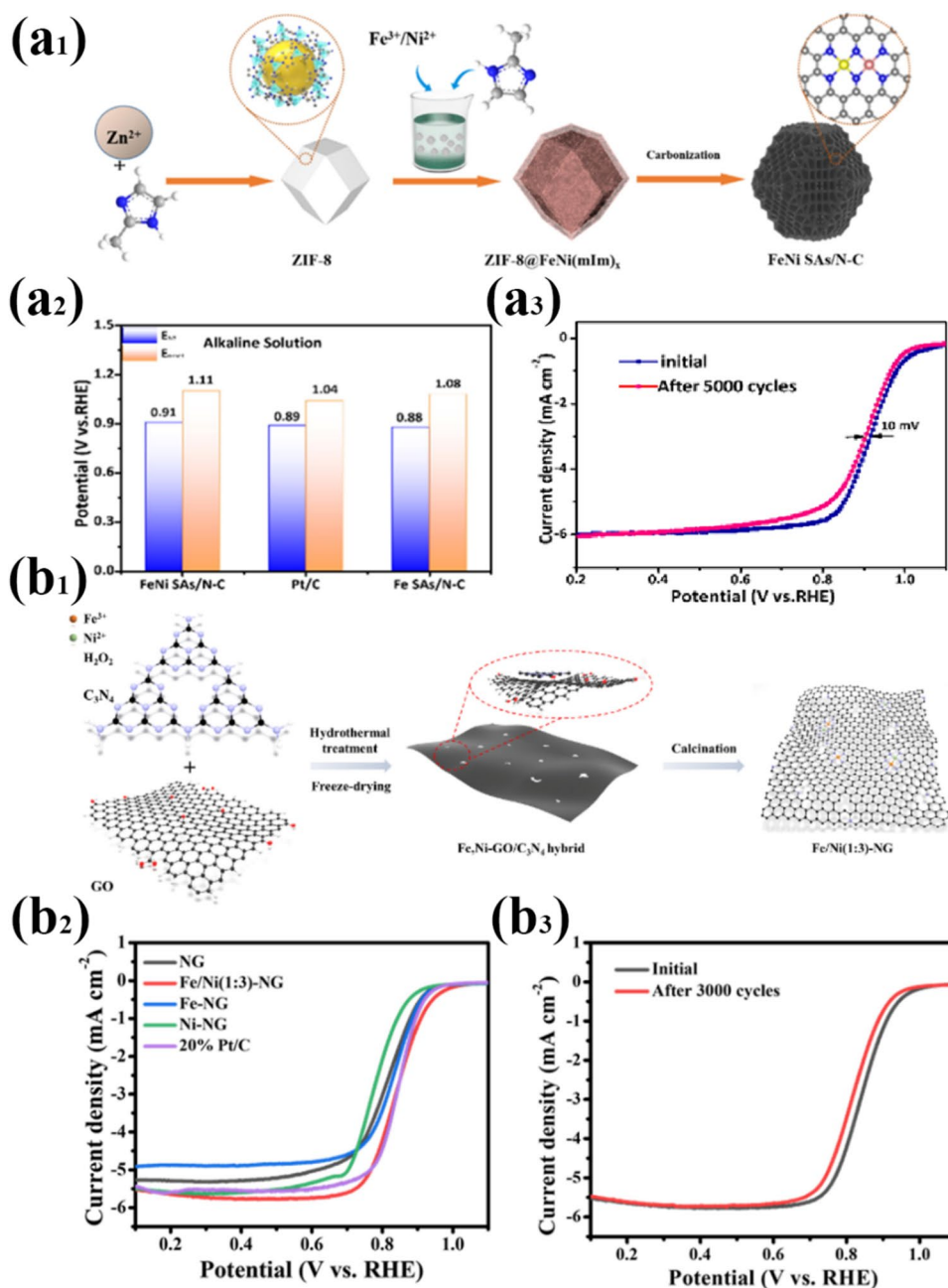
are still some disadvantages that are difficult to avoid [158]. It is easy to cause the migration of active components during drying [159].

Atomic layer deposition

Researchers found that atomic deposition layer (ALD) can effectively avoid migration of active sites via depositing atoms on the carrier in the atmosphere of vapor phase. As a kind of gas-phase deposition strategy, ALD can deposit single atoms layer by layer on the surface of supports [160, 161]. This is an effective strategy to control SACs based on atomic scaling.

As a case, Kim et al. [162] prepared Pt_3Ti SACs via the coupled of ALD with thermal reductive annealing. This affinity ensured that Pt and TiO_2 were in close contact due to the strong metal support interaction between Pt and TiO_2. As-synthesized Pt_3Ti SACs showed excellent specific activity 5.3-fold higher than Pt/C. Jiao et al. [163] fabricated MoS_2-NTA with different nanotube diameters and wall thicknesses by a sacrificial strategy of anodic aluminum oxide template via ALD. Then, Pt atoms were fixed on the wall of Ti_3C_2-supported MoS_2-NTA (Fig. 17a1). The abundant defects on Pt/MoS_2-NTA/Ti_3C_2 (Fig. 17a2) and individual Pt atoms on the MoS_2-NTA

Fig. 15 a_1 Illustration of FeCo-N-C; a_2 ORR curves recorded in O_2-saturated 0.1 M KOH [61]. Copyright 2021, American Chemical Society. b_1 Illustration of FeCo-NC; b_2 The ORR polarization profiles of the samples; b_3 Tafel curves of FeCo-NC and Pt/C [63]. Copyright 2021, Wiley.
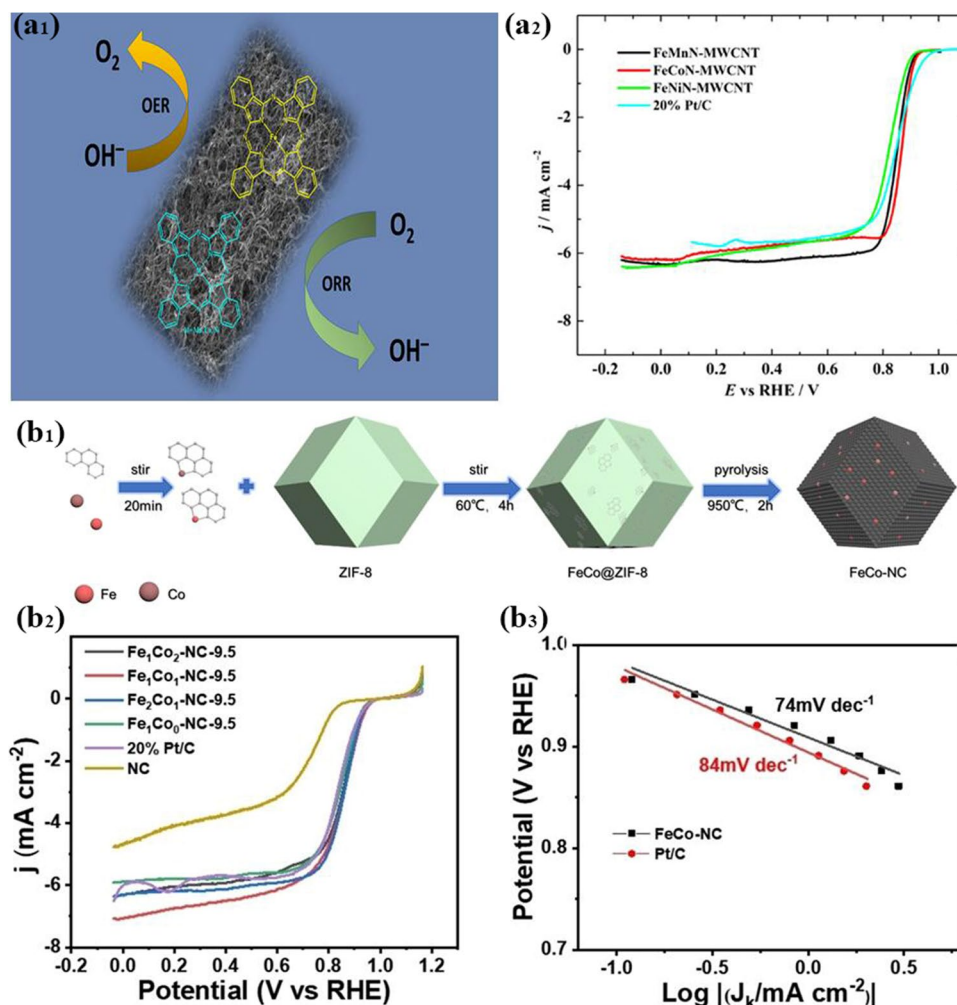
surface (Fig. 17a3) are beneficial for enhancing the catalytic efficiency. Wang et al. [164] reported Fe SACs supported on the substrates of multiwalled carbon nanotubes, SiO_2, and TiO_2 with the Fe loading of > 1.5 wt% via ALD (Fig. 17b1), as shown in Fig. 17b2-3.

ALD can precisely control the growth of atoms in a single metal on the carrier, so such technology has been used to study the growth mechanism and the influence during the formation processes of isolated metal atoms. However, although ALD method has been used, the shortcomings of time-consuming and high requirements for material properties still exist [165].

High-temperature pyrolysis

For reducing the time, high-temperature pyrolysis method has attracted the attention of researchers. It is a method to generate target SACs by heating functional organic structure with suitable metal elements at high temperature, displaying the advantages of simple operation, rapid response, and easy

adjustment [166]. At present, high-temperature pyrolysis has been widely used [167, 168].

For instance, Chen et al. [169] synthesized Fe/Co–N–C by a water-regulated and bioinspired one-step pyrolysis method at 800 °C (Fig. 18a1-2). Through pyrolysis, single atoms were coated on carbon nanotubes, so that the large specific surface area and porous structure of the catalyst template can be fully utilized. It made the catalyst have higher activity and stable. Ding et al. [170] reported the preparation of thermally stable metal oxide–supported Pt SAC by flame spray pyrolysis (Fig. 18b1). The results revealed that flame spray pyrolysis favored the formation of tetragonal-monoclinic phase of ZrO_2 with improved redox property, thus leading to enhanced catalytic activity in high-temperature applications (Fig. 18b2).

In addition, taking MOF as a precursor and then pyrolysis is also a common synthetic method. Xie et al. [171] synthesized Fe SAC via pyrolysis a mesoporous cage architecture (Fig. 18c1). The catalysts exhibited an $E_{1/2}$ of 0.94 V (Fig. 18c2) and good durability (Fig. 18c3). Yaengthip et al. [173] prepared N-doped reduced graphene oxide by
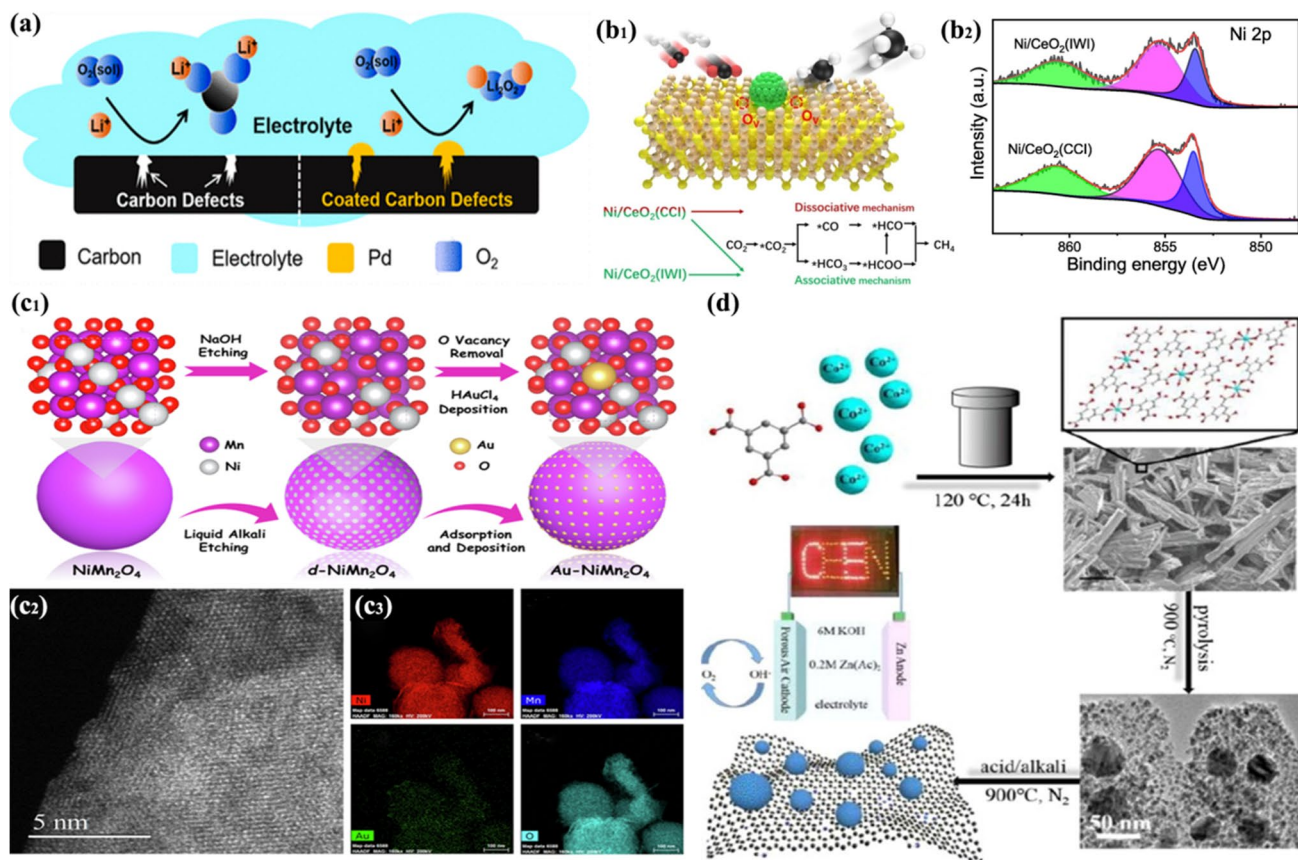
Fig. 16 a Schematic of the Pd/carbon cathode architecture [151]. Copyright 2019, American Chemical Society. **b₁** Ni/CeO₂(CCI) Concept Schematic; **b₂** Ni 2p spectra of Ni/CeO₂(IWI) and Ni/CeO₂(CCI) [152]. Copyright 2022, Elsevier. **c₁** The synthesis procedure of Aux-NiMn₂O₄; **c₂** HAADF-STEM image and **c₃** EDS mapping of Au₀.₁₂-NiMn₂O₄ [154]. Copyright 2022, Elsevier. **d** Schematic diagram of Co-SAC synthesis [155]. Copyright 2018, Elsevier.
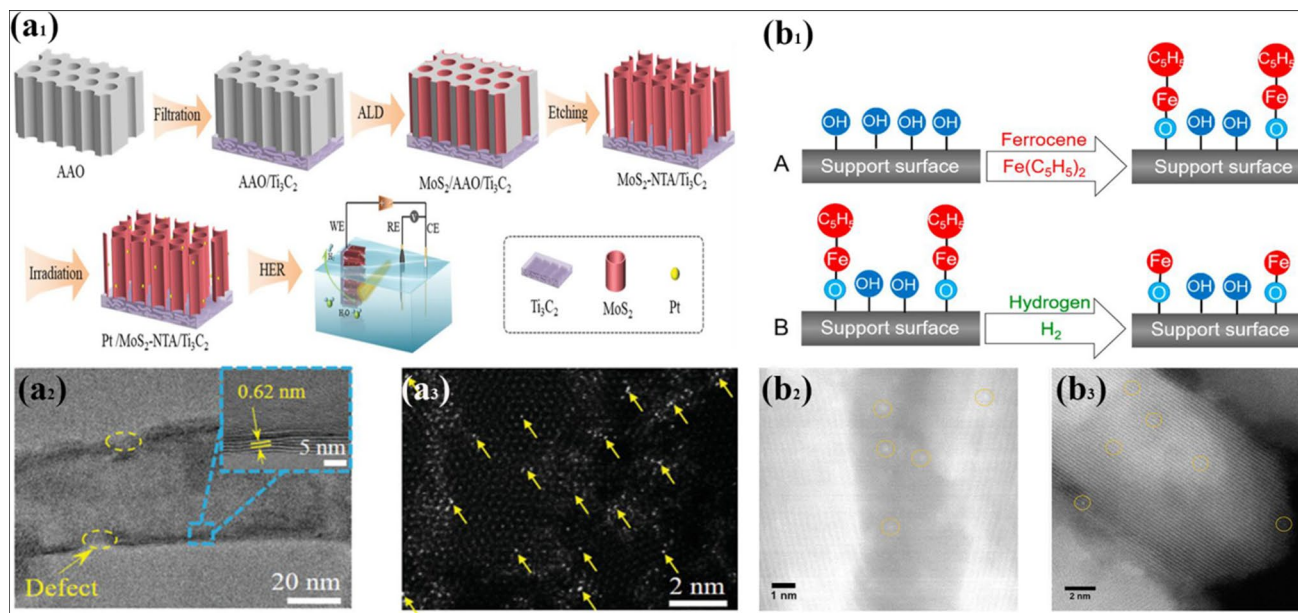
Fig. 17 a₁ The synthesis processes of Pt/MoS₂-NTA/Ti₃C₂; **a₂** HRTEM image of the single MoS₂ nanotube in Pt/MoS₂-NTA/Ti₃C₂; the inset: partial enlargement displaying the MoS₂ interlayer spacing; **a₃** the HAADF-STEM images of Pt/MoS₂-NTA [163]. Copyright 2022, Elsevier. **b₁** Scheme for Fe ALD half-reactions; HAADF-STEM images of **b₂** 10c-Fe/MWCNTs and **b₃** 15c-Fe/TiO₂ samples [164]. Copyright 2020, American Chemical Society.
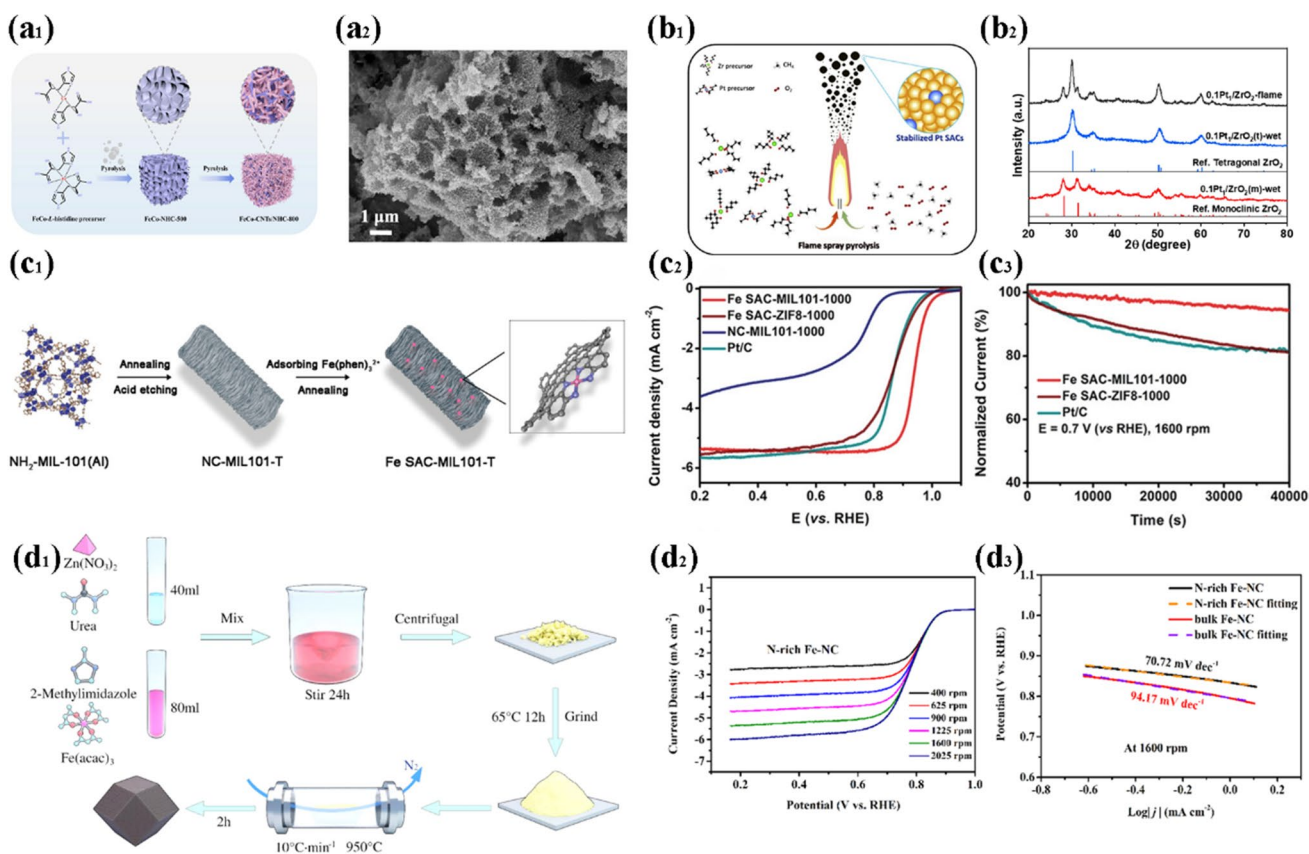
Fig. 18 a_1 Schematic of FeCo-CNTs/NHC; a_2 SEM of FeCo-CNTs/NHC-800 [169]. Copyright 2022, Elsevier. b_1 Schematic of Pt SAC; b_2 XRD pattern of Pt SAC [170]. Copyright 2021, Elsevier. c_1 Illustration for the preparation of Fe SAC-MIL101-T; c_2 LSV curves; c_3 normalized I–T curves of Fe SAC-MIL101-T [171]. Copyright 2021, Wiley. d_1 The synthesis strategy of N-rich Fe-NC; d_2 LSV curves; d_3 Tafel plots of N-rich Fe-NC [172]. Copyright 2021, Elsevier.

pyrolysis with urea as N_2 source. Then, by controlling the temperature, different N contents of SACs are achieved, which showed higher ORR activity and they had outstanding durability and stability after running within saturated oxygen for over 2000 cycles. Xu et al. [174] developed a rapid and solvent-free method to produce Fe-doped ZIF-8 under microwave irradiation. After rational pyrolysis, Fe–N–C was obtained. The catalysts exhibited an E_{onset} of 0.884 V and an $E_{1/2}$ of 0.782 V. Chen et al. [172] employed urea as a dispersant and as an additional nitrogen source to synthesize ZIF-8-derived Fe–N–C (Fig. 18d1). The catalyst showed an E_{onset} of 0.91 V (Fig. 18d2) and J_L of 5.38 mA cm^{-2} (Fig. 18d3).

A series of SACs prepared by the high-temperature pyrolysis has been reported. However, it is limited by the choice of the metal precursor ligands and carrier, being accessible to residual during the process of pyrolysis. Moreover, isolated atoms with high surface free energy are easy to agglomeration at high temperature, reducing the catalytic activity.

Others

Furthermore, there are many other ways to synthesize SACs such as chemical vapor deposition (CVD), Lewis acid, and ball milling. For example, Liu et al. [175] synthesized Fe–N–C with FeN_4 sites using CVD technology. Zhong et al. [176] prepared the single-atom Fe on wood-based porous carbon via Lewis acid pretreatment and carbonization. Lewis acid $FeCl_3$ pretreatment not only produced abundant microchannels but also introduced Fe–N species, enhancing the ORR performance and durability. Jin et al. [177] reported a rapid and straightforward method to construct K_2PtCl_4@NC-M by the spherical grinding of Pt precursors and N-doped carbon carriers. Many Pt atoms are dispersed on NC through ball milling conducive to improving ORR performance. However, most of these methods are still in the initial experimental stage, and further research is still necessary.

Conclusion and outlook

In summary, we presented a comprehensive study on the progress of SACs for ORR, including noble metal SACs, transition metal SACs, single-atom alloy SACs, and double metal SACs, as well as discussed several common synthesis methods. For noble metal SACs, their electrocatalytic activity is higher than that of transition metal SACs, but the limited resources and poor durability lead to difficult application widely. About transition metal SACs, they have sufficient resources and excellent stability, but the issues of low catalyst performance and low metal loading still need to be solved. The single-atom alloy SACs have unique electronic structures and well-defined active sites, but complex synthesis methods and mechanisms still need to be improved and explored. About double metal SACs, they possess higher metal loading and better performance compared to transition metal SACs. But the metal atom aggregation is still a big challenge. In order to accurately preparing SACs, some synthesis methods are often used. In terms of wet chemistry, it can inhibit metal aggregation during the preparation process and effectively improve the utilization rate of atoms. But it is easy to cause the migration of active site during drying. ALD can effectively avoid metal atom aggregation and control the metal atoms on the carrier. However, it also has the shortcoming of time-consuming and high requirements for material properties. In addition, high-temperature pyrolysis is a method with the advantages of simple operation, rapid response, and easy adjustment. But its high surface free energy of the isolated atoms is easy to agglomerate at high temperature.

To obtain the high-performance SACs based on the recent progresses, the following research directions should be considered: (1) improving the dispersion and loading of metal active centers by regulating the coordination structure of metal atoms, such as S and P participating in metal atom coordination; (2) exploring suitable carriers involving coordination controllability of metal active centers, abundance of raw materials, and structural stability; (3) combining the advantages of different synthesis methods while avoiding their disadvantages to achieve the efficient synthesis of SACs; (4) further clarifying the synergistic mechanism between metal atoms in SACs containing two and/or more metal active centers to guide the active center regulation.

Data Availability The data that support the findings of this study are available.

References

1. Zhao YM, Zhang PC, Xu C, Zhou XY, Liao LM, Wei PJ, Liu E, Chen H, He Q, Liu JG (2020) Design and preparation of Fe-N$_5$ catalytic sites in single-atom catalysts for enhancing the oxygen reduction reaction in fuel cells. ACS Appl Mater Interfaces 12(15):17334–17342

2. Zhang S, Ao X, Huang J, Wei B, Zhai Y, Zhai D, Deng W, Su C, Wang D, Li Y (2021) Isolated single-atom Ni-N$_5$ catalytic site in hollow porous carbon capsules for efficient lithium-sulfur batteries. Nano Lett 21(22):9691–9698

3. Xu Y, Gong H, Song L, Kong Y, Jiang C, Xue H, Li P, Huang X, He J, Wang T (2022) A highly efficient and free-standing copper single atoms anchored nitrogen-doped carbon nanofiber cathode toward reliable Li–CO$_2$ batteries. Mater Today Ener 25:100967

4. Xu X, Wang S, Guo S, San Hui K, Ma J, Dinh DA, Hui KN, Wang H, Zhang L, Zhou G (2022) Cobalt phosphosulfide nanoparticles encapsulated into heteroatom-doped carbon as bifunctional electrocatalyst for Zn–air battery. Adv Powder Mater 1(3):100027

5. Yu D, Ma Y, Hu F, Lin CC, Li L, Chen HY, Han X, Peng S (2021) Dual-sites coordination engineering of single atom catalysts for flexible metal–air batteries. Adv Energy Mater 11(30):2101242

6. Xu X, Hui KS, Hui KN, Shen J, Zhou G, Liu J, Sun Y (2021) Engineering strategies for low-cost and high-power density aluminum-ion batteries. Chem Eng J 418(15):129385

7. Cheng Y, Zhou S, Wang R, Gao X, Zhang Y, Xiang Z (2021) A superior unitary oxygen electrode with accelerated mass transfer and highly exposed active sites for rechargeable air-based batteries. J Power Sources 488:229468

8. Guo D, Shibuya R, Akiba C, Saji S, Kondo T, Nakamura J (2016) Active sites of nitrogen-doped carbon materials for oxygen reduction reaction clarified using model catalysts. Science 351(6271):361–365

9. Gawish MA, Drmosh QA, Onaizi SA (2022) Single atom catalysts: an overview of the coordination and interactions with metallic supports. Chem Rec 22(7):e202100328

10. Qi P, Wang J, Djitcheu X, He D, Liu H, Zhang Q (2022) Techniques for the characterization of single atom catalysts. RSC Adv 12:1216–1227

11. Xu X, Zhao X, Hui KS, Dinh DA, Hui KN (2021) Rechargeable batteries: regulating electronic and ionic transports for high electrochemical performance. Adv Mater Technol 7(5):2101107

12. Xu M, Lai C, Liu X, Li B, Zhang M, Xu F, Liu S, Li L, Qin L, Yi H, Fu Y (2021) COF-confined catalysts: from nanoparticles and nanoclusters to single atoms. J Mater Chem A 9:24148–24174

13. Liu X, Zhang G, Wang L, Fu H (2021) Structural design strategy and active site regulation of high-efficient bifunctional oxygen reaction electrocatalysts for Zn-air battery. Small 17(48):e2006766

14. Lai WH, Zhang BW, Hu Z, Qu XM, Jiang YX, Wang YX, Wang JZ, Liu HK, Chou SL (2019) The quasi-Pt-allotrope catalyst: hollow PtCo@single-atom Pt$_1$ on nitrogen-doped carbon toward superior oxygen reduction. Adv Func Mater 29(13):1807340

15. Tong M, Wang L, Fu H (2021) Designed synthesis and catalytic mechanisms of non-precious metal single-atom catalysts for oxygen reduction reaction. Small Methods 5(10):2100865

16. Chen J-J, Gu S, Hao R, Wang Z-Y, Li M-Q, Li Z-Q, Liu K, Liao K-M, Wang Z-Q, Huang H, Li Y-Z, Zhang K-L, Lu Z-G (2022) Co single atoms and nanoparticles dispersed on N-doped carbon nanotube as high-performance catalysts for Zn-air batteries. Rare Met 41:2055–2062

17. Xiaoqin X, Jiahao X, Bin L, Rongyue W, Mingyang L, Jun Z, Jin L, Zhuang C, Jinlong Z (2022) PBA-derived FeCo alloy with

core-shell structure embedded in 2D N-doped ultrathin carbon sheets as a bifunctional catalyst for rechargeable Zn-air batteries. Appl Catal B 316:121687

18. Wang M, Zhang H, Liu Y, Pan Y (2022) Research progress of precise structural regulation of single atom catalyst for accelerating electrocatalytic oxygen reduction reaction. J Ener Chem 72:56–72

19. Qingyun Q, Shufang J, Yuanjun C, Dingsheng W, Yadong L (2021) Design and structural engineering of single-atomic-site catalysts for acidic oxygen reduction reaction. Trend Chem 3(11):954–968

20. Han X, Ling X, Yu D, Xie D, Li L, Peng S, Zhong C, Zhao N, Deng Y, Hu W (2019) Atomically dispersed binary Co-Ni sites in nitrogen-doped hollow carbon nanocubes for reversible oxygen reduction and evolution. Adv Mater 31(49):e1905622

21. Guo J, Liu H, Li D, Wang J, Djitcheu X, He D, Zhang Q (2022) A minireview on the synthesis of single atom catalysts. RSC Advances 12:9373–9394

22. Gawande MB, Ariga K, Yamauchi Y (2021) Single-atom catalysts, Advanced Materials. Interfaces 8(8):2100436

23. Lin J, Chen X, Zheng Y, Xiao Y, Zheng Y, Jiang L (2022) Sulfur-resistant methane combustion invoked by surface property regulation on palladium-based catalysts. Appl Surf Sci 587:152835

24. Morales-Leal FJ, Rivera De la Rosa J, Lucio-Ortiz CJ, De Haro Del DA, Río MA, Garza-Navarro W, Tian JEH (2021) Monometallic platinum and palladium–based catalysts in the competitive oxidation of methanol over the liquid–phase methanol–ethanol mixtures. Chem Eng J 426:131623

25. Zhao W, Wang J, Yin R, Li B, Huang X, Zhao L, Qian L (2020) Single-atom Pt supported on holey ultrathin g-C_3N_4 nanosheets as efficient catalyst for Li-O_2 batteries. J Colloid Interface Sci 564:28–36

26. Fan M, Cui J, Zhang J, Wu J, Chen S, Song L, Wang Z, Wang A, Vajtai R, Wu Y, Ajayan PM, Jiang J, Sun D (2021) The modulating effect of N coordination on single-atom catalysts researched by Pt-N-C model through both experimental study and DFT simulation. J Mater Sci Technol 91:160–167

27. Weikai X, Yonghui Z, Zheng J, Xiaopeng L, Hao Z, Yu S, Zhijun N, Fuping D, Peng G, Jing Q, Kenichi K, Miho Y, Yuhan S (2018) Palladium single atoms supported by interwoven carbon nanotube and manganese oxide nanowire networks for enhanced electrocatalysis†. J Mater Chem A 18:5067–5073

28. Meng Y, Li J-C, Zhao S-Y, Shi C, Li X-Q, Zhang L, Hou P-X, Liu C, Cheng H-M (2021) Fluorination-assisted preparation of self-supporting single-atom Fe-N-doped single-wall carbon nanotube film as bifunctional oxygen electrode for rechargeable Zn-Air batteries. Appl Catal B 294:120239

29. Cai S, Cheng Y, Meng Z, Li G, Wu J, Kan E, Ouyang B, Zhang H, Tang H (2022) The design of single iron atoms dispersed with nitrogen coordination environment electrocatalyst for zinc-air battery. J Power Sources 529:231174

30. Han J, Bao H, Wang J-Q, Zheng L, Sun S, Wang ZL, Sun C (2021) 3D N-doped ordered mesoporous carbon supported single-atom Fe-N-C catalysts with superior performance for oxygen reduction reaction and zinc-air battery. Appl Catal B 280:119411

31. Cao Y, Peng H, Chu S, Tang Y, Huang C, Wang Z, Liu F, Wu J, Shan B, Chen R (2021) Molten-salt-assisted thermal emitting method to transform bulk Fe_2O_3 into Fe single atom catalysts for oxygen reduction reaction in Zn-air battery. Chem Eng J 420:129713

32. Han J, Meng X, Lu L, Bian J, Li Z, Sun C (2019) Single-atom Fe-N_x-C as an efficient electrocatalyst for zinc–air batteries. Adv Func Mater 29(41):1808872

33. Chen K, Kim S, Je M, Choi H, Shi Z, Vladimir N, Kim KH, Li OL (2021) Ultrasonic plasma engineering toward facile synthesis of single-atom M-N_4/N-doped carbon (M=Fe, Co) as

superior oxygen electrocatalyst in rechargeable zinc-air batteries. Nanomicro Lett 13(1):60

34. Guo J, Yan X, Liu Q, Li Q, Xu X, Kang L, Cao Z, Chai G, Chen J, Wang Y, Yao J (2018) The synthesis and synergistic catalysis of iron phthalocyanine and its graphene-based axial complex for enhanced oxygen reduction. Nano Energy 46:347–355

35. Wu D, Hu J, Zhu C, Zhang J, Jing H, Hao C, Shi Y (2021) Salt melt synthesis of Chlorella-derived nitrogen-doped porous carbon with atomically dispersed CoN_4 sites for efficient oxygen reduction reaction. J Colloid Interface Sci 586:498–504

36. Xu Z, Zhu J, Shao J, Xia Y, Tseng J, Jiao C, Ren G, Liu P, Li G, Chen R, Chen S, Huang F, Wang H-L (2022) Atomically dispersed cobalt in core-shell carbon nanofiber membranes as super-flexible freestanding air-electrodes for wearable Zn-air batteries. Energy Storage Mater 47:365–375

37. Xu R, Wang X, Zhang C, Zhang Y, Jiang H, Wang H, Su G, Huang M, Toghan A (2022) Engineering solid–liquid-gas interfaces of single-atom cobalt catalyst for enhancing the robust stability of neutral Zn-air batteries under high current density. Chem Eng J 433:133685

38. Yang H, Gao S, Rao D, Yan X (2022) Designing superior bifunctional electrocatalyst with high-purity pyrrole-type CoN_4 and adjacent metallic cobalt sites for rechargeable Zn-air batteries. Energy Storage Mater 46:553–562

39. Luo F, Zhu J, Ma S, Li M, Xu R, Zhang Q, Yang Z, Qu K, Cai W, Chen Z (2021) Regulated coordination environment of Ni single atom catalyst toward high-efficiency oxygen electrocatalysis for rechargeable zinc-air batteries. Energy Storage Mater 35:723–730

40. Qiu HJ, Du P, Hu K, Gao J, Li H, Liu P, Ina T, Ohara K, Ito Y, Chen M (2019) Metal and nonmetal codoped 3D nanoporous graphene for efficient bifunctional electrocatalysis and rechargeable Zn-air batteries. Adv Mater 31(19):e1900843

41. Zhao S, Cheng Y, Veder J-P, Johannessen B, Saunders M, Zhang L, Liu C, Chisholm MF, De Marco R, Liu J, Yang S-Z, Jiang SP (2018) One-pot pyrolysis method to fabricate carbon nanotube supported Ni single-atom catalysts with ultrahigh loading. ACS Appl Energy Mater 1:5286–5297

42. Yang J, Liu W, Xu M, Liu X, Qi H, Zhang L, Yang X, Niu S, Zhou D, Liu Y, Su Y, Li JF, Tian ZQ, Zhou W, Wang A, Zhang T (2021) Dynamic behavior of single-atom catalysts in electrocatalysis: identification of Cu-N_3 as an active site for the oxygen reduction reaction. J Am Chem Soc 143(36):14530–14539

43. Gu L, Dong Y, Du H, Zhang Y, Yuan Q, Wang B, Wang H, Zhao J, Zhang N (2020) Preparation and characterization of nitrogen-riched polymer based materials and the role of Cu–N active site in promoting the ORR activity of the catalyst. Catal Surv Asia 24(3):219–231

44. Han G, Zheng Y, Zhang X, Wang Z, Gong Y, Du C, Banis MN, Yiu Y-M, Sham T-K, Gu L, Sun Y, Wang Y, Wang J, Gao Y, Yin G, Sun X (2019) High loading single-atom Cu dispersed on graphene for efficient oxygen reduction reaction. Nano Energy 66:104088

45. Jiang R, Chen X, Liu W, Wang T, Qi D, Zhi Q, Liu W, Li W, Wang K, Jiang J (2021) Atomic Zn sites on N and S codoped biomass-derived graphene for a high-efficiency oxygen reduction reaction in both acidic and alkaline electrolytes. ACS Appl Ener Mater 4(3):2481–2488

46. Wang N, Liu Z, Ma J, Liu J, Zhou P, Chao Y, Ma C, Bo X, Liu J, Hei Y, Bi Y, Sun M, Cao M, Zhang H, Chang F, Wang H-L, Xu P, Hu Z, Bai J, Sun H, Hu G, Zhou M (2020) Sustainability perspective-oriented synthetic strategy for zinc single-atom catalysts boosting electrocatalytic reduction of carbon dioxide and oxygen. ACS Sustain Chem Eng 8(36):13813–13822

47. Li J, Chen S, Yang N, Deng M, Ibraheem S, Deng J, Li J, Li L, Wei Z (2019) Ultrahigh-loading zinc single-atom catalyst for

highly efficient oxygen reduction in both acidic and alkaline media. Angew Chem Int Ed Engl 58(21):7035–7039

48. Wang J, Li H, Liu S, Hu Y, Zhang J, Xia M, Hou Y, Tse J, Zhang J, Zhao Y (2021) Turning on Zn 4s electrons in a N_2-Zn-B_2 configuration to stimulate remarkable ORR performance. Angew Chem Int Ed Engl 60(1):181–185

49. Zhiyu L, Hao H, Ling C, Yang Y, Ruirui Z, Qianwang C (2019) Atomically dispersed Mn within carbon frameworks as high-performance oxygen reduction electrocatalysts for zinc–air battery. ACS Sustain Chem Eng 8(1):427–434

50. Yan L, Xie L, Wu XL, Qian M, Chen J, Zhong Y, Hu Y (2021) Precise regulation of pyrrole-type single-atom Mn-N_4 sites for superior pH-universal oxygen reduction. Carbon Energy 3(6):856–865

51. Sahoo L, Garg R, Kaur K, Vinod CP, Gautam UK (2022) Ultrathin twisty PdNi alloy nanowires as highly active ORR electrocatalysts exhibiting morphology-induced durability over 200 K cycles. Nano Lett 22(1):246–254

52. Betancourt LE, Rojas-Pérez A, Orozco I, Frenkel AI, Li Y, Sasaki K, Senanayake SD, Cabrera CR (2020) Enhancing ORR performance of bimetallic PdAg electrocatalysts by designing interactions between Pd and Ag. ACS Applied Energy Materials 3(3):2342–2349

53. Kim D-H, Lee E, Pak C (2021) Effect of rare-earth elements in Pd ternary alloy catalysts on activity toward oxygen reduction reaction. Catal Today 359:106–111

54. Bai J, Ge W, Zhou P, Xu P, Wang L, Zhang J, Jiang X, Li X, Zhou Q, Deng Y (2022) Precise constructed atomically dispersed Fe/Ni sites on porous nitrogen-doped carbon for oxygen reduction. J Colloid Interface Sci 616:433–439

55. Liu J, Fan C, Liu G, Jiang L (2021) MOF-derived dual metal (Fe, Ni)–nitrogen–doped carbon for synergistically enhanced oxygen reduction reaction. Appl Surf Sci 538:148017

56. Wang H, Su S, Yu T, Meng C, Zhou H, Zhao W, Yan S, Bian T, Yuan A (2022) FeNi/$NiFe_2O_4$ hybrids confined in N-doped carbon sponge derived from Hofmann-type MOFs for oxygen electrocatalysis. Appl Surf Sci 596:153522

57. Ma Y, Fan H, Wu C, Zhang M, Yu J, Song L, Li K, He J (2021) An efficient dual-metal single-atom catalyst for bifunctional catalysis in zinc-air batteries. Carbon 185:526–535

58. Zhang C, Wu C, Gao Y, Gong Y, Liu H, He J (2021) FeNi nanoparticles coated on N-doped ultrathin graphene-like nanosheets as stable bifunctional catalyst for Zn-air batteries. Chem Asian J 16(12):1592–1602

59. Wu Y, Ye C, Yu L, Liu Y, Huang J, Bi J, Xue L, Sun J, Yang J, Zhang W, Wang X, Xiong P, Zhu J (2022) Soft template-directed interlayer confinement synthesis of a Fe-Co dual single-atom catalyst for Zn-air batteries. Energy Storage Mater 45:805–813

60. Liu J, He T, Wang Q, Zhou Z, Zhang Y, Wu H, Li Q, Zheng J, Sun Z, Lei Y, Ma J, Zhang Y (2019) Confining ultrasmall bimetallic alloys in porous N–carbon for use as scalable and sustainable electrocatalysts for rechargeable Zn–air batteries. J Mater Chem A 7(20):12451–12456

61. Kumar Y, Kibena-Põldsepp E, Kozlova J, Rahn M, Treshchalov A, Kikas A, Kisand V, Aruvali J, Tamm A, Douglin JC, Folkman SJ, Gelmetti I, Garces-Pineda FA, Galan-Mascaros JR, Dekel DR, Tammeveski K (2021) Bifunctional oxygen electrocatalysis on mixed metal phthalocyanine-modified carbon nanotubes prepared via pyrolysis. ACS Appl Mater Interfaces 13(35):41507–41516

62. Yu K, Shi P-H, Fan J-C, Min Y-L, Xu Q-J (2019) Porous Fe Co, and N-co-doped carbon nanofibers as high-efficiency oxygen reduction catalysts. J Nanopart Res 21(11):230

63. Zhou M, Zhu Z, Ju Y, Zhai Y, Jiao L, Liu M, Yang W, Tang J (2022) Bimetallic FeCo–N–C catalyst for efficient oxygen reduction reaction. Electroanalysis 34:1–8

64. Lai WH, Zhang L, Yan Z, Hua W, Indris S, Lei Y, Liu H, Wang YX, Hu Z, Liu HK, Chou S, Wang G, Dou SX (2021) Activating inert surface Pt single atoms via subsurface doping for oxygen reduction reaction. Nano Lett 21(19):7970–7978

65. Xiang Z, Li W, Liu F, Tan F, Han F, Wang X, Shao C, Xu M, Liu W, Yang X (2021) Catalyst with a low load of platinum and high activity for oxygen reduction derived from strong adsorption of Pt–N_4 moieties on a carbon surface. Electrochem Commun 127:107039

66. Kim HE, Lee IH, Cho J, Shin S, Ham HC, Kim JY, Lee H (2019) Palladium single-atom catalysts supported on C@C_3N_4 for electrochemical reactions. ChemElectroChem 6(18):4757–4764

67. Cheng X, Wang Y, Lu Y, Zheng L, Sun S, Li H, Chen G, Zhang J (2022) Single-atom alloy with Pt-Co dual sites as an efficient electrocatalyst for oxygen reduction reaction. Appl Catal B 306(5):121112

68. Lee W-J, Bera S, Woo H-J, Hong W, Park J-Y, Oh S-J, Kwon S-H (2022) Atomic layer deposition enabled PtNi alloy catalysts for accelerated fuel-cell oxygen reduction activity and stability. Chem Eng J 442:136123

69. Liu J, Lan J, Yang L, Wang F, Yin J (2019) PtM (M=Fe Co, Ni) Bimetallic nanoclusters as active, methanol-tolerant, and stable catalysts toward the oxygen reduction reaction. ACS Sustain Chem Eng 7(7):6541–6549

70. Li X, Liu Y, Zhu J, Tsiakaras P, Shen PK (2022) Enhanced oxygen reduction and methanol oxidation reaction over self-assembled Pt-M (M=Co, Ni) nanoflowers. J Colloid Interface Sci 607(Pt2):1411–1423

71. Peng L, Shang L, Zhang T, Waterhouse GIN (2020) Recent advances in the development of single-atom catalysts for oxygen electrocatalysis and zinc–air batteries. Adv Energy Mater 10(48):2003018

72. Jeong YS, Park JB, Jung HG, Kim J, Luo X, Lu J, Curtiss L, Amine K, Sun YK, Scrosati B, Lee YJ (2015) Study on the catalytic activity of noble metal nanoparticles on reduced graphene oxide for oxygen evolution reactions in lithium-air batteries. Nano Lett 15(7):4261–4268

73. Fung V, Hu G, Tao FF, Jiang D-E (2019) Methane chemisorption on oxide-supported Pt single atom. ChemPhysChem 20(17):2217–2220

74. Wan Q, Fung V, Lin S, Wu Z, Jiang D-E (2020) Perovskite-supported Pt single atoms for methane activation. J Mater Chem A 8:4362–4368

75. Han B, Guo Y, Huang Y, Xi W, Xu J, Luo J, Qi H, Ren Y, Liu X, Qiao B, Zhang T (2020) Strong metal-support interactions between Pt single atoms and TiO_2. Angew Chem Int Ed 59(29):11824–11829

76. Zengxi W, Bowen D, Peng C, Teng Z, Shuangliang Z (2021) Palladium-based single atom catalysts for high-performance electrochemical production of hydrogen peroxide. Chem Eng J 428:131112

77. Xiang C, Liu Q, Shi L, Liu Z (2020) Radical-assisted formation of Pd single atoms or nanoclusters on biochar. Front Chem 8:598352

78. Strasser JW, Crooks RM (2022) Single atoms and small clusters of atoms may accompany Au and Pd dendrimer-encapsulated nanoparticles. Soft Matter 18:5067–5073

79. Wang N, Zhao X, Zhang R, Yu S, Levell ZH, Wang C, Ma S, Zou P, Han L, Qin J, Ma L, Liu Y, Xin HL (2022) Highly selective oxygen reduction to hydrogen peroxide on a carbon-supported single-atom Pd electrocatalyst. ACS Catal 12(7):4156–4164

80. Qin Z, Zhao J (2022) 1 T-$MoSe_2$ monolayer supported single Pd atom as a highly-efficient bifunctional catalyst for ORR/OER. J Colloid Interface Sci 605:155–162

81. Fortunato GV, Bezerra LS, Cardoso ESF, Kronka MS, Santos AJ, Greco AS, Junior JLR, Lanza MRV, Maia G (2022) Using

palladium and gold palladium nanoparticles decorated with molybdenum oxide for versatile hydrogen peroxide electroproduction on graphene nanoribbons. ACS Appl Mater Interfaces 14(5):6777–6793

82. Vega-Cartagena M, Rojas-Pérez A, Colón-Quintana GS, Blasini Pérez DA, Peña-Duarte A, Larios-Rodríguez E, De Jesús MA, Cabrera CR (2021) Potential dependent Ag nanoparticle electrodeposition on Vulcan XC-72R carbon support for alkaline oxygen reduction reaction. J Electroanalytic Chem 891:115242

83. Xiao M, Zhu J, Li G, Li N, Li S, Cano ZP, Ma L, Cui P, Xu P, Jiang G, Jin H, Wang S, Wu T, Lu J, Yu A, Su D, Chen Z (2019) A single-atom iridium heterogeneous catalyst in oxygen reduction reaction. Angew Chem Int Ed Engl 58(28):9640–9645

84. Xu F, Wang D, Sa B, Yu Y, Mu S (2017) One-pot synthesis of Pt/CeO$_2$/C catalyst for improving the ORR activity and durability of PEMFC. Int J Hydrogen Energy 42(18):13011–13019

85. Roh C-W, Choi J, Lee H (2018) Hydrophilic-hydrophobic dual catalyst layers for proton exchange membrane fuel cells under low humidity. Electrochem Commun 97:105–109

86. Zhao L, Xinhua L, Jingrui T, Yingmei Z, Wenchang Z (2021) Nonmetal-doping of noble metal-based catalysts for electrocatalysis. Nanoscale 13:11314–11324

87. Li M, Wang H, Luo W, Sherrell PC, Chen J, Yang J (2020) Heterogeneous single-atom catalysts for electrochemical CO$_2$ reduction reaction. Adv Mater 32(34):e2001848

88. Liang Z, Shen J, Xu X, Li F, Liu J, Yuan B, Yu Y, Zhu M (2022) Advances in the development of single-atom catalysts for high-energy-density lithium-sulfur batteries. Adv Mater 34:e2200102

89. Deng L, Qiu L, Hu R, Yao L, Zheng Z, Ren X, Li Y, He C (2022) Restricted diffusion preparation of fully-exposed Fe single-atom catalyst on carbon nanospheres for efficient oxygen reduction reaction. Appl Catal B 305:121058

90. Hu S, Ni W, Yang D, Ma C, Zhang J, Duan J, Gao Y, Zhang S (2020) Fe$_3$O$_4$ nanoparticles encapsulated in single-atom Fe–N–C towards efficient oxygen reduction reaction: effect of the micro and macro pores. Carbon 162:245–255

91. Gong X-F, Zhang Y-L, Zhao L, Dai Y-K, Cai J-J, Liu B, Guo P, Zhou Q-Y, Yagi I, Wang Z-B (2022) Zinc/graphitic carbon nitride co-mediated dual-template synthesis of densely populated Fe–N$_x$-embedded 2D carbon nanosheets towards oxygen reduction reactions for Zn–air batteries. J Mater Chem A 10(11):5971–5980

92. Lu C, Chen Y, Yang Y, Chen X (2020) Single-atom catalytic materials for lean-electrolyte ultrastable lithium-sulfur batteries. Nano Lett 20(7):5522–5530

93. Zhang W, Wang L, Zhang LH, Chen D, Zhang Y, Yang D, Yan N, Yu F (2022) Creating hybrid coordination environment in Fe-based single atom catalyst for efficient oxygen reduction. Chemsuschem 15(12):e202200195

94. Chen Z, Song J, Peng X, Xi S, Liu J, Zhou W, Li R, Ge R, Liu C, Xu H, Zhao X, Li H, Zhou X, Wang L, Li X, Zhong L, Rykov AI, Wang J, Koh MJ, Loh KP (2021) Iron single atom catalyzed quinoline synthesis. Adv Mater 33(34):e2101382

95. Liu Q, Wang Y, Hu Z, Zhang Z (2021) Iron-based single-atom electrocatalysts: synthetic strategies and applications. RSC Adv 11(5):3079–3095

96. Yang S, Zhang T, Li G, Yang L, Lee JY (2017) Facile synthesis of N/M/O (M=Fe Co, Ni) doped carbons for oxygen evolution catalysis in acid solution. Ener Stor Mater 6:140–148

97. Liang X, Li Z, Xiao H, Zhang T, Xu P, Zhang H, Gao Q, Zheng L (2021) Two types of single-atom FeN$_4$ and FeN$_5$ electrocatalytic active centers on N-doped carbon driving high performance of the SA-Fe-NC oxygen reduction reaction catalyst. Chem Mater 33(14):5542–5554

98. Zhong X, Yi W, Qu Y, Zhang L, Bai H, Zhu Y, Wan J, Chen S, Yang M, Huang L, Gu M, Pan H, Xu B (2020) Co single-atom anchored on Co$_3$O$_4$ and nitrogen-doped active carbon toward bifunctional catalyst for zinc-air batteries. Appl Catal B 260:118188

99. Li H, Zhang M, Zhou W, Duan J, Jin W (2021) Ultrathin 2D catalysts with N-coordinated single Co atom outside Co cluster for highly efficient Zn-air battery. Chem Eng J 421:129719

100. Lian Z, Lu Y, Wang C, Zhu X, Ma S, Li Z, Liu Q, Zang S (2021) Single-atom Ru implanted on Co$_3$O$_4$ nanosheets as efficient dual-catalyst for Li-CO$_2$ batteries. Adv Sci (Weinh) 8(23):e2102550

101. Seyed Ali M, Mehdi M (2021) Fabrication of copper centered metal organic framework and nitrogen, sulfur dual doped graphene oxide composite as a novel electrocatalyst for oxygen reduction reaction. Energy 214:119053

102. Taotao Z, Yanling Q, Pengfei Y, Xianfeng L, Huamin Z (2019) Bi-modified Zn catalyst for efficient CO$_2$ electrochemical reduction to formate. ACS Sustain Chem Eng 7(18):15190–15196

103. Jie G, Chunlei W, Mei D, Guofu W, Zhikai L, Zhangfeng Q, Jianguo W, Weibin F (2019) Evolution of Zn species on Zn/HZSM-5 catalyst under H$_2$ pretreated and its effect on ethylene aromatization. Chem Cat Chem 11(16):3892–3902

104. Lingzhe M, Erhuan Z, Haoyu P, Yu W, Dingsheng W, Hongpan R, Jiatao Z (2022) Bi/Zn dual single-atom catalysts for electroreduction of CO$_2$ to syngas. Chem Cat Chem 14(7):e202101801

105. Junqing L, Yu Z, Mingyuan Z, Lihua K (2020) A density functional theory exploration on the Zn catalyst for acetylene hydration. J Mol Model 26:105

106. Zhen M, Vusala AA, Dilgam BT, Fedor IZ, Firudin IG, Kamran TM, Armando JLP (2020) Multinuclear Zn(II)-arylhydrazone complexes as catalysts for cyanosilylation of aldehydes. J Organomet Chem 912:121171

107. Haijuan Z, Xiaoyan S, Bin T, Gang W, Baojun M, Wanyi L (2020) The performance of Cu/Zn/Zr catalysts of different Zr/(Cu+Zn) ratio for CO$_2$ hydrogenation to methanol. Catal Commun 149:106264

108. Hao Z, Chen J, Zhang D, Zheng L, Li Y, Yin Z, He G, Jiao L, Wen Z, Lv X-J (2021) Coupling effects of Zn single atom and high curvature supports for improved performance of CO$_2$ reduction. Sci Bullet 66(16):1649–1658

109. Song CL, Li ZH, Ma LY, Li MZ, Huang S, Hong XJ, Cai YP, Lan YQ (2021) Single-atom zinc and anionic framework as janus separator coatings for efficient inhibition of lithium dendrites and shuttle effect. ACS Nano 15(8):13436–13443

110. Kexi L, Zhi Q, Sooyeon H, Zhenyu L, Hanguang Z, Dong S, Hui X, Gang W, Guofeng W (2018) Mn- and N-doped carbon as promising catalysts for oxygen reduction reaction: theoretical prediction and experimental validation. Appl Catal B 243:195–203

111. Tian Z, Bikun Z, Qiong P, Jian Z, Zhimei S (2020) Mo$_2$B$_2$ MBene-supported single-atom catalysts as bifunctional HER/OER and OER/ORR electrocatalysts. J Mater Chem A 1(159):433–441

112. Qiangqiang G (2020) A DFT study of the ORR on M-N3 (M = Mn, Fe Co, Ni, or Cu) co-doped graphene with moiety-patched defects. Ionics 26:2453–2465

113. Guangqi Z, Fan L, Yicheng W, Zidong W, Wei W (2019) Systematic exploration of N, C coordination effects on the ORR performance of Mn–$_N$x doped graphene catalysts based on DFT calculations†. Phys Chem Chem Phys 21:12826–12836

114. Liu H, Zhu S, Cui Z, Li Z, Wu S, Liang Y (2021) Boosting oxygen reduction catalysis with abundant single atom tin active sites in zinc-air battery. J Power Sources 490:229483

115. Luo E, Zhang H, Wang X, Gao L, Gong L, Zhao T, Jin Z, Ge J, Jiang Z, Liu C, Xing W (2019) Single-atom Cr-N$_4$ sites designed for durable oxygen reduction catalysis in acid media. Angew Chem Int Ed 131(36):12599–12605

116. Xue Z, Zhang X, Qin J, Liu R (2021) Anchoring Mo on C_9N_4 monolayers as an efficient single atom catalyst for nitrogen fixation. J Ener Chem 57:443–450

117. Da Y, Jiang R, Tian Z, Han X, Chen W, Hu W (2022) The applications of single-atom alloys in electrocatalysis: progress and challenges. Smart Mat 18. https://doi.org/10.1002/smm2.1136

118. Wu D, Shen X, Pan Y, Yao L, Peng Z (2020) Platinum alloy catalysts for oxygen reduction reaction: advances, challenges and perspectives. Chem Nano Mat 6(1):32–41

119. Wu D, Shen X, Pan Y, Yao L, Peng Z (2019) Platinum alloy catalysts for oxygen reduction reaction: advances, challenges and perspectives. Chem Nano Mat 6(1):32–41

120. Zhang L, Liu H, Liu S, Norouzi Banis M, Song Z, Li J, Yang L, Markiewicz M, Zhao Y, Li R, Zheng M, Ye S, Zhao Z-J, Botton GA, Sun X (2019) Pt/Pd single-atom alloys as highly active electrochemical catalysts and the origin of enhanced activity. ACS Catalysis 9(10):9350–9358

121. Swami A, Patil I, Lokanathan M, Ingavale S, Kakade B (2020) Enhanced oxygen reduction reaction by Pd-Pt alloy catalyst with stabilized platinum skin. Chem Select 5(12):3486–3493

122. Jiang J, Ding W, Li W, Wei Z (2020) Freestanding single-atom-layer pd-based catalysts: oriented splitting of energy bands for unique stability and activity. Chem 6(2):431–447

123. Nam G, Park J, Choi M, Oh P, Park S, Kim MG, Park N, Cho J, Lee J-S (2015) Carbon-coated core–shell Fe–Cu nanoparticles as highly active and durable electrocatalysts for a Zn–Air battery. ACS Nano 9(6):6493–6501

124. Niu L, Liu G, Li Y, An J, Zhao B, Yang J, Qu D, Wang X, An L, Sun Z (2021) CoNi alloy nanoparticles encapsulated in N-doped graphite carbon nanotubes as an efficient electrocatalyst for oxygen reduction reaction in an alkaline medium. ACS Sustain Chem Eng 9(24):8207–8213

125. Chen W, Yu H, Chang S, Li W, Liu R, Wang Y, Zhang H, Zhang Z (2022) Wheat straw as carbon source to prepare $FeCoP_2$/N, P dual-doped carbon matrix as bifunctional catalyst for application in rechargeable zinc-air and aluminum-air batteries. Appl Surf Sci 573:151486

126. Lei L, Yameng L, Tao Z, Rao H, Xinrui C, Tiane F, Yuhua W (2022) Exploring highly efficient dual-metal-site electrocatalysts for oxygen reduction reaction by first principles screening. J Electrochem Soc 169:026524

127. Zou W, Lu R, Liu X, Xiao G, Liao X, Wang Z, Zhao Y (2022) Theoretical insights into dual-atom catalysts for the oxygen reduction reaction: the crucial role of orbital polarization. J Mater Chem A 10:9150–9160

128. Pedersen A, Barrio J, Li A, Jervis R, Brett DJL, Titirici MM, Stephens IEL (2021) Dual-metal atom electrocatalysts: theory, synthesis, characterization, and applications. Adv Energy Mater 12(3):2102715

129. Zhang J, Huang Q-A, Wang J, Wang J, Zhang J, Zhao Y (2020) Supported dual-atom catalysts: preparation, characterization, and potential applications. Chin J Catal 41(5):783–798

130. Liu J, Cao D, Xu H, Cheng D (2020) From double-atom catalysts to single-cluster catalysts: a new frontier in heterogeneous catalysis. Nano Select 2(2):251–270

131. Li Z, Ren Q, Wang X, Chen W, Leng L, Zhang M, Horton JH, Liu B, Xu Q, Wu W, Wang J (2021) Highly active and stable palladium single-atom catalyst achieved by a thermal atomization strategy on an SBA-15 molecular sieve for semi-hydrogenation reactions. ACS Appl Mater Interfaces 13(2):2530–2537

132. Zhifu W, Ya-Qiong S, Emiel JMH, Xinlong T, Chenghang Y, Qin X (2019) Highly stable Pt_3Ni nanowires tailored with trace Au for the oxygen reduction reaction. J Mater Chem A 7:26402–26409

133. Wan XK, Samjeske G, Matsui H, Chen C, Muratsugu S, Tada M (2021) Ultrafine Pt-Ni nanoparticles in hollow porous carbon spheres for remarkable oxygen reduction reaction catalysis. Dalton Trans 50(20):6811–6822

134. Li K, Zhang H, Zheng Y, Yuan G, Jia Q, Zhang S (2020) Catalytic preparation of carbon nanotubes from waste polyethylene using FeNi bimetallic nanocatalyst. Nanomaterials 10(8):1517

135. Xie D, Yu D, Hao Y, Han S, Li G, Wu X, Hu F, Li L, Chen HY, Liao YF, Peng S (2021) Dual-active sites engineering of N-doped hollow carbon nanocubes confining bimetal alloys as bifunctional oxygen electrocatalysts for flexible metal–air batteries. Small 17(10):2007239

136. Li X, Su Z, Zhao Z, Cai Q, Li Y, Zhao J (2021) Single Ir atom anchored in pyrrolic-N_4 doped graphene as a promising bifunctional electrocatalyst for the ORR/OER: a computational study. J Colloid Interface Sci 607:1005–1013

137. Sirirak R, Jarulertwathana B, Laokawee V, Susingrat W, Sarakonsri T (2016) FeNi alloy supported on nitrogen-doped graphene catalysts by polyol process for oxygen reduction reaction (ORR) in proton exchange membrane fuel cell (PEMFC) cathode. Res Chem Intermed 43(5):2905–2919

138. Liu Y, Wu X, Guo X, Lee K, Sun Q, Li X, Zhang C, Wang Z, Hu J, Zhu Y, Leung MKH, Zhu Z (2020) Modulated FeCo nanoparticle in situ growth on the carbon matrix for high-performance oxygen catalysts. Mater Today Ener 19:100610

139. Samad S, Loh KS, Wong WY, Sudarsono W, Lee TK, Wan Daud WR (2020) Effect of various Fe/Co ratios and annealing temperatures on a Fe/Co catalyst supported with nitrogen-doped reduced graphene oxide towards the oxygen reduction reaction. J Alloys Compounds 816:152573

140. Parkash A, Jia Z, Tian T, Ge Z, Yu C, Chunli X (2020) A new generation of platinum-copper electrocatalysts with ultra-low concentrations of platinum for oxygen-reduction reactions in alkaline media. Chem Select 5(11):3391–3397

141. Xu J, Lai S, Qi D, Hu M, Peng X, Liu W, Liu W, Hu G, Xu H, Li F, Li C, He J, Zhuo L, Sun J, Qiu Y, Zhang S, Luo J, Liu X (2021) Atomic Fe-Zn dual-metal sites for high-efficiency pH-universal oxygen reduction catalysis. Nano Res 14(5):1374–1381

142. Gharibi H, Dalir N, Jafari M, Parnian MJ, Zhiani M (2022) Engineering dual metal single-atom sites with the nitrogen-coordinated nonprecious catalyst for oxygen reduction reaction (ORR) in acidic electrolyte. Appl Surf Sci 572:151367

143. Shah SSA, Najam T, Javed MS, Bashir MS, Nazir MA, Khan NA, Rehman AU, Subhan MA, Rahman MM (2021) Recent advances in synthesis and applications of single-atom catalysts for rechargeable batteries. Chem Rec 22(7):e202100280

144. Zhu Y, Peng W, Li Y, Zhang G, Zhang F, Fan X (2019) Modulating the electronic structure of single-atom catalysts on 2D nanomaterials for enhanced electrocatalytic performance. Small Methods 3(9):1800438

145. Lin L, Chen Z, Chen W (2021) Single atom catalysts by atomic diffusion strategy. Nano Res 14:4398–4416

146. Zhang L, Zhao X, Yuan Z, Wu M, Zhou H (2021) Oxygen defect-stabilized heterogeneous single atom catalysts: preparation, properties and catalytic application. J Mater Chemis A 9:3855–3879

147. Xue K, Mo Y, Long B, Wei W, Shan C, Guo S, Niu L (2022) Single-atom catalysts supported on ordered porous materials: synthetic strategies and applications. Info Mat 4(6):e12296

148. Sołtys-Mróz M, Syrek K, Pierzchała J, Wiercigroch E, Malek K, Sulka GD (2020) Band gap engineering of nanotubular Fe_2O_3-TiO_2 photoanodes by wet impregnation. Appl Surf Sci 517:146195

149. Thayagaraja R, Cheng SY, Jones MI, Baroutian S (2020) Catalytic wet oxidation of glucose as model compound of wastewater over copper/rare earth oxides catalysts. J Water Process Eng 36:101251

150. Li X, Wang Z, Feng R, Huang J, Fang Y (2021) A novel approach to prepare efficient CO_2 sorbents derived from alumina-extracted residue of coal ash. J Environ Chem Eng 9(6):106373

151. Zhang T, Zou B, Bi X, Li M, Wen J, Huo F, Amine K, Lu J (2019) Selective growth of a discontinuous subnanometer Pd film on carbon defects for Li–O$_2$ batteries. ACS Energy Lett 4(12):2782–2786

152. Zou X, Shen Z, Li X, Cao Y, Xia Q, Zhang S, Liu Y, Jiang L, Li L, Cui L, Wang Y (2022) Boosting CO$_2$ methanation on ceria supported transition metal catalysts via chelation coupled wetness impregnation. J Colloid Interface Sci 620:77–85

153. Yi M, Li N, Lu B, Li L, Zhu Z, Zhang J (2021) Single-atom Pt decorated in heteroatom (N, B, and F)-doped ReS$_2$ grown on Mo$_2$CT$_x$ for efficient pH-universal hydrogen evolution reaction and flexible Zn–air batteries. Energy Storage Mater 42:418–429

154. Qin M, Fan S, Li X, Tade MO, Liu S (2022) Electroreductive CO coupling of benzaldehyde over SACs Au-NiMn$_2$O$_4$ spinel synergetic composites. J Colloid Interface Sci 625:305–316

155. Lu H-S, Zhang H, Zhang X, Sun N, Zhu X, Zhao H, Wang G (2018) Transformation of carbon-encapsulated metallic Co into ultrafine Co/CoO nanoparticles exposed on N-doped graphitic carbon for high-performance rechargeable zinc-air battery. Appl Surf Sci 448:369–379

156. Keller L, Ohs B, Lenhart J, Abduly L, Blanke P, Wessling M (2018) High capacity polyethylenimine impregnated microtubes made of carbon nanotubes for CO$_2$ capture. Carbon 126:338–345

157. Salehi S, Anbia M (2018) Highly efficient CO$_2$ capture with a metal–organic framework-derived porous carbon impregnated with polyethyleneimine. Appl Organomet Chem 32(7):e4390

158. Slyemi S, Barama S, Barama A, Blanchard J, Messaoudi H, Casale S, Calers C (2018) Characterization and reactivity of VMgO catalysts prepared by wet impregnation and sol–gel methods. Chem Eng Commun 205(9):1288–1298

159. Eskandari S, Tate G, Leaphart NR, Regalbuto JR (2018) Nanoparticle synthesis via electrostatic adsorption using incipient wetness impregnation. ACS Catal 8(11):10383–10391

160. Beshkova M, Deminskyi P, Hsu CW, Shtepliuk I, Avramova I, Yakimova R, Pedersen H (2021) Atomic layer deposition of AlN on graphene Physica Status Solidi (A) -. Appl Mater Sci 218(17):2000684

161. Liu Z, Andrade AM, Grewal S, Nelson AJ, Thongrivong K, Kang H-S, Li H, Nasef Z, Diaz G, Lee MH (2021) Trace amount of ceria incorporation by atomic layer deposition in Co/CoO$_x$-embedded N-doped carbon for efficient bifunctional oxygen electrocatalysis: demonstration and quasi-operando observations. Int J Hydrogen Energy 46(77):38258–38269

162. Kim Y, Xu S, Park J, Dadlani AL, Vinogradova O, Krishnamurthy D, Orazov M, Lee DU, Dull S, Schindler P, Han HS, Wang Z, Graf T, Schladt TD, Mueller JE, Sarangi R, Davis R, Viswanathan V, Jaramillo TF, Higgins DC, Prinz FB (2022) Improving intrinsic oxygen reduction activity and stability: atomic layer deposition preparation of platinum-titanium alloy catalysts. Appl Catal B 300:120741

163. Jiao S, Kong M, Hu Z, Zhou S, Xu X, Liu L (2022) Pt atom on the wall of atomic layer deposition (ALD)-made MoS$_2$ nanotubes for efficient hydrogen evolution. Small 18(16):2105129

164. Wang X, Jin B, Jin Y, Wu T, Ma L, Liang X (2020) Supported single Fe atoms prepared via atomic layer deposition for catalytic reactions. ACS Appl Nano Mater 3(3):2867–2874

165. Lee M, Ahmad W, Kim DW, Kwon KM, Kwon HY, Jang H-B, Noh S-W, Kim D-H, Zaidi SJA, Park H, Lee HC, Abdul Basit M, Park TJ (2022) Powder coatings via atomic layer deposition for batteries: a review. Chem Mater 34(8):3539–3587

166. Ko K-H, Park T-J, Sahajwalla V, Rawal A (2021) Complex microstructural evolution in high temperature pyrolysis of plastic and biomass. Fuel 291:120153

167. Che Y, Wang Q, Huo J, Tian Y (2021) Determination of the sensitive fractions for vacuum residue high temperature fast pyrolysis. Fuel 299:120903

168. Shen J, Wen Y, Jiang H, Yu S, Dong C, Fan Y, Liu B, Li C (2022) Identifying activity trends for the electrochemical production of H$_2$O$_2$ on M-N–C single-atom catalysts using theoretical kinetic computations. J Physic Chem C 126(25):10388–10398

169. Chen YP, Zhang L, Feng JJ, Li XS, Wang AJ (2022) Water-regulated and bioinspired one-step pyrolysis of iron-cobalt nanoparticles-capped carbon nanotubes/porous honeycombed nitrogen-doped carbon composite for highly efficient oxygen reduction. J Colloid Interface Sci 618:352–361

170. Ding S, Chen H-A, Mekasuwandumrong O, Hülsey MJ, Fu X, He Q, Panpranot J, Yang C-M, Yan N (2021) High-temperature flame spray pyrolysis induced stabilization of Pt single-atom catalysts. Appl Catal B 281:199471

171. Xie X, Peng L, Yang H, Waterhouse GIN, Shang L, Zhang T (2021) MIL-101-derived mesoporous carbon supporting highly exposed Fe single-atom sites as efficient oxygen reduction reaction catalysts. Adv Mater 33(23):e2101038

172. Zhe-qin C, Xiao-cong Z, Yong-min X, Jia-ming L, Zhi-feng X, Rui-xiang W (2021) A high-performance nitrogen-rich ZIF-8-derived Fe-NC electrocatalyst for the oxygen reduction reaction. J Alloy Compd 884:160980

173. Yaengthip P, Siyasukh A, Payattikul L, Kiatsiriroat T, Punyawudho K (2022) The ORR activity of nitrogen doped-reduced graphene oxide below decomposition temperature cooperated with cobalt prepared by strong electrostatic adsorption technique. J Electroanal Chem 915:116366

174. Xu X, Zhang X, Xia Z, Sun R, Li H, Wang J, Yu S, Wang S, Sun G (2021) Solid phase microwave-assisted fabrication of Fe-doped ZIF-8 for single-atom Fe-N-C electrocatalysts on oxygen reduction. J Ener Chem 54:579–586

175. Liu S, Wang M, Yang X, Shi Q, Qiao Z, Lucero M, Ma Q, More KL, Cullen DA, Feng Z, Wu G (2020) Chemical vapor deposition for atomically dispersed and nitrogen coordinated single metal site catalysts. Angew Chem Int Ed Engl 59(48):21698–21705

176. Zhong L, Jiang C, Zheng M, Peng X, Liu T, Xi S, Chi X, Zhang Q, Gu L, Zhang S, Shi G, Zhang L, Wu K, Chen Z, Li T, Dahbi M, Alami J, Amine K, Lu J (2021) Wood carbon based single-atom catalyst for rechargeable Zn–Air batteries. ACS Energy Lett 6(10):3624–3633

177. Jin H, Sultan S, Ha M, Tiwari JN, Kim MG, Kim KS (2020) Simple and scalable mechanochemical synthesis of noble metal catalysts with single atoms toward highly efficient hydrogen evolution. Adv Func Mater 30(25):2000531